TU Delft

Delft University of Technology

Document Version
Final published version

Licence
Dutch Copyright Act (Article 25fa)

Citation (APA)
Schoenborn, S., Lloyd, T., Sivakumaran, Y., Woodruff, M. A., Fletcher, D. F., Pirola, S., & Allenby, M. C. (2026). Haemodynamic impact of implant materials and anastomotic angle in femoro-popliteal artery grafts. *Biomechanics and Modeling in Mechanobiology*, *25*(1), Article 17. https://doi.org/10.1007/s10237-025-02037-3

Important note
To cite this publication, please use the final published version (if applicable).
Please check the document version above.

Copyright
In case the licence states “Dutch Copyright Act (Article 25fa)”, this publication was made available Green Open Access via the TU Delft Institutional Repository pursuant to Dutch Copyright Act (Article 25fa, the Taverne amendment). This provision does not affect copyright ownership.
Unless copyright is transferred by contract or statute, it remains with the copyright holder.

Sharing and reuse
Other than for strictly personal use, it is not permitted to download, forward or distribute the text or part of it, without the consent of the author(s) and/or copyright holder(s), unless the work is under an open content license such as Creative Commons.

Takedown policy
Please contact us and provide details if you believe this document breaches copyrights.
We will remove access to the work immediately and investigate your claim.

This work is downloaded from Delft University of Technology.

Biomechanics and Modeling in Mechanobiology (2026) 25:17
https://doi.org/10.1007/s10237-025-02037-3

ORIGINAL PAPER

Haemodynamic impact of implant materials and anastomotic angle in femoro-popliteal artery grafts

Sabrina Schoenborn[1] · Thomas Lloyd[2] · Yogeesan Sivakumaran[3] · Maria A. Woodruff[4] · David F. Fletcher[5] · Selene Pirola[6] · Mark C. Allenby[1]

Received: 7 May 2025 / Accepted: 13 October 2025
© The Author(s), under exclusive licence to Springer-Verlag GmbH Germany, part of Springer Nature 2026

Abstract

End-to-side anastomoses are commonly utilised in peripheral arterial bypass surgery and are plagued by high rates of re-stenosis which are contributed to by non-physiological blood flow impacting the arterial and graft structures. Computational simulations can examine how patient-specific surgical decisions in bypass graft placement and material selection affect blood flow and future risk of graft restenosis. Despite graft geometry and compliance being key predictors of restenosis, current simulations of femoro-popliteal artery grafts do not consider the interaction of flowing blood with compliant vessel, graft, and suture structures. Utilising fluid–structure interaction simulations, this study examines the impact of surgical technique, such as anastomosis angle, graft material, and suture material, on blood flow and fluid–structure forces in patient-specific asymptomatic arterial tree versus side-to-end peripheral grafts for symptomatic atherosclerotic disease. To render these complex simulations numerically feasible, our pipeline uses regional suture mechanics and a pre-stress pipeline previously validated in small-scale idealised models. Our simulations found that higher anastomosis angles generate larger regions of slow and recirculating blood, characterised by non-physiologically low shear stress and high oscillatory shear index. The use of compliant graft materials reduces regions of non-physiologically high shear stress only when used in combination with compliant suture materials. Altogether, our fluid–structure interaction simulation provides patient-specific platforms for vascular surgery decisions concerning graft geometry and material.

Keywords Peripheral artery disease · Blood flow · Computational fluid dynamics · Fluid–structure interaction · Cardiovascular biomechanics

✉ Mark C. Allenby
m.allenby@uq.edu.au

Sabrina Schoenborn
sabrina@schoenborn.tech

Thomas Lloyd
thomas.lloyd@health.qld.gov.au

Yogeesan Sivakumaran
yogeesan.sivakumaran@health.qld.gov.au

Maria A. Woodruff
mia.woodruff@qut.edu.au

David F. Fletcher
david.fletcher@sydney.edu.au

Selene Pirola
s.pirola@tudelft.nl

[1] BioMimetic Systems Engineering (BMSE) Lab, School of Chemical Engineering, University of Queensland (UQ), St Lucia, QLD 4072, Australia

[2] Department of Diagnostic Radiology, Princess Alexandra Hospital, Woolloongabba, QLD 4102, Australia

[3] Department of Vascular Surgery, Princess Alexandra Hospital, Woolloongabba, QLD 4102, Australia

[4] Biofabrication and Tissue Morphology (BTM) Lab, School of Mechanical, Medical and Process Engineering, Centre of Biomedical Technologies, Queensland University of Technology, Kelvin Grove, QLD 4072, Australia

[5] School of Chemical and Biomolecular Engineering, University of Sydney, Darlington, NSW 2006, Australia

[6] Department of Biomechanical Engineering, Faculty of Mechanical Engineering, Delft University of Technology, Delft, The Netherlands

Published online: 13 January 2026

1 Introduction

Cardiovascular disease (CVD) is the most common cause of death worldwide. The annual incidence of global deaths related to CVD is expected to rise from 16.7 million in 2002 to 23.3 million in 2030 (D. and Loncar, C. Mathers 2002). A common manifestation of CVD is peripheral arterial disease (PAD), whose symptoms develop as a consequence of the critical atherosclerotic narrowing of the peripheral arteries. International research studies show a prevalence of approximately 10–20% for PAD depending on study design, country, and participant's age and gender (Bauersachs et al. 2019). PAD affects more than 200 million people worldwide, with atherosclerosis accounting for more than 90% of cases of PAD. In Australian primary care settings, up to 15% of patients have a diagnosis of PAD (Conte and Vale 2018). This study focuses on the femoro-popliteal segment, since it is the arterial segment with the highest likelihood to develop PAD (Kasapis and Gurm 2010; Aronow 2007) with the femoral and popliteal arteries being affected in 80–90% of symptomatic PAD patients (Shu and Santulli 2018).

In the case of PAD progression to critical limb threatening ischaemia (CLTI), restoration of tissue perfusion is essential for limb salvage. Current revascularisation techniques consist of endovascular interventions, including angioplasty, stenting and other endovascular adjuncts (atherectomy and catheter directed thrombolysis), as well as open surgical repair with bypass grafting using autologous or prosthetic conduit. The choice of operative treatment for CLTI has been evaluated recently in the BASIL-2 and Best-CLI trials which demonstrated disparate results when comparing open versus endovascular revascularisation techniques for CLTI (Bradbury et al. 2023; Farber et al. 2022). From the perspective of lower limb bypass surgery, the gold standard conduit is autologous, with the great saphenous vein demonstrating the best patency rates at all intervals and the fewest re-interventions (Klinkert et al. 2003). Great saphenous vein as a bypass graft conduit has an average primary patency rates of 74% after 5 years (Klinkert et al. 2004). However, the use of autologous grafts require harvesting and may be unavailable for use as a result of prior bypass grafting procedures or pre-existing conditions (varicose degeneration) (Stewart and Lyman 2004). One-third of patients requiring primary revascularisation lack a suitable autologous conduit. This number increases to 50% in patients presenting for a re-operation or secondary bypass procedure (Carrabba and Madeddu 2018).

In cases where no autologous graft can be used, blood flow can be restored by implanting synthetic grafts. The two most common materials for synthetic vascular grafts are expanded poly(tetrafluoroethylene) (ePTFE) and poly(ethylene terephthalate) (PET), better known by its brand name Dacron® (Walpoth and Bowlin 2005). While synthetic grafts are readily accessible in all required lengths and diameters, their low average primary patency rates of 39% after 5 years are their most significant limitation (Klinkert et al. 2004). The economic burden associated with PAD is considerable because of the high rates of leg revascularisation procedures and hospitalisations (Mahoney et al. 2010) and the poorer results of secondary bypass surgeries that may be required after primary bypass graft failure (Lepäntalo et al. 2012).

While early graft failure within 30 days of bypass grafting is usually due to complications at the time of surgery, such as technical errors, graft thrombogenicity, low flow, or poor run-off, late graft failure is mainly caused by the graft abnormality and metachronous disease. In particular, graft stenoses due to intimal hyperplasia (Thomas et al. 2013; Bregy et al. 2008; Conte et al. 2002; D.N. and F. 2013) at points of anastomosis have been reported as a major cause of failure in autogenous and prosthetic bypass (Stewart and Lyman 2004; D.N. and F. 2013; Sottiurai et al. 1983; Taylor et al. 1987).

Intimal hyperplasia (IH) is the chronic and excessive thickening of the tunica intima, caused by abnormal proliferation and migration of vascular smooth muscle cells (VSMCs) in response to endothelial injury or dysfunction with associated deposition of connective extracellular matrix (ECM), which results in either partial or complete occlusion of the blood vessel (Graham et al. 1992; Tiwari et al. 2003; Brody and Pickering 1989). IH leads to graft failure due to restenosis in approximately 20–30% of femoro-distal bypasses utilising autologous conduit and is recognised as the main cause of thrombotic complications occurring between 2 and 24 months after a vascular intervention (Lemson et al. 2000). Current surgical anastomotic interventions for vascular anastomoses utilise a monofilament suture, with a continuous polypropylene (Prolene®) suture being considered the gold standard. Regardless of the choice of suture material and technique, suturing results in injury of the vessel wall and the presence of foreign material at the blood-graft interface (Tiwari et al. 2003).

A range of biological, chemical, and mechanical factors have been studied with regards to their potential to aggravate the severity of IH (Jeong et al. 2020), and compliance mismatch of graft and anastomosis with the host artery is one of the central biomechanical issues of vascular graft design, as greater compliance mismatch is associated with greater incidence and severity of IH and consequently lower mid-term patency rates (Lemson et al. 2000; Post et al. 2019).

Combined in vivo and in-silico studies on small-diameter arterial models have demonstrated that the severity of IH is related to local biomechanical factors. In particular,

regions most significantly affected by femoro-popliteal artery IH are the toe, heel, and floor of the anastomosis (Meyerson et al. 2001; Schoenborn et al. 2022). The sudden change in flow direction at the anastomosis site induces regions of both high and low wall shear stress (WSS) and disturbed flow profiles, including secondary, recirculating, and oscillatory flows (D.N. and F. 2013). Both the magnitude and the level of flow disturbance as marked by the oscillatory shear index have been indicated to affect IH severity (Jia et al. 2015). Additionally, high intramural stresses at the suture line due to the presence of stiff graft and suture materials have been indicated to have a proliferative effect on IH around the suture (Trubel et al. 1995), with the degree of IH linked to the mechanical compliance mismatch between the connected materials (Post et al. 2019). Similar flow phenomena have been simulated in other small-diameter artery grafts, including AV fistulae (Jodko and Barber 2024; Colley et al. 2022; Quicken et al. 2020; Bozzetto et al. 2016; Ngoepe et al. 2011) and venous and arterial coronary grafts (Ramachandra et al. 2016) which generate regions of low blood pressure, low and oscillating blood flow, and low wall shear stress, hypothesised to contribute to patient IH and restenosis.

Two-way coupled fluid–structure interaction (FSI) simulations are particularly useful where changes in vascular compliance, which may occur during disease or after surgical intervention, are of interest. Since rigid-wall fluid dynamics simulations are shown to overestimate WSS by 10–15% in cardiovascular applications (McGah et al. 2014; Decorato et al. 2011, 2014; Lopes et al. 2019), FSI approaches have become increasingly well-used. Examples of FSI applications are studies on the increase in stroke work after aortic aneurysm repair with a stiff graft (Bakel et al. 2019), the effect of graft versus stent repair on haemodynamics (Jayendiran et al. 2018a), vascular wall stress profiles after aortic grafting (Jayendiran et al. 2018b), the identification of adverse oscillatory flow after implantation of stiff Dacron® grafts (Tubaldi et al. 2018), the investigation of suitable graft materials for aortic repair (Rahmani et al. 2017), the effect of different surgical orientations and graft length ratios on haemodynamics (G. E. et al.. 2018), and the prediction of rupture risk in cerebral aneurysms (Cho et al. 2020).

Due to the complex fluid and structural mechanics contributing to IH in femoro-popliteal artery grafts, this study aims to analyse both the geometric factors, such as anastomosis angle, and the structural factor, such as choice of suture and graft material, by independently utilising a multi-patient and asymptomatic femoro-popliteal artery graft FSI study.

2 Methods

An FSI model coupling blood flow with artery, graft, and suture wall motion was developed using the 2023R1 version of the commercial computational software suite Ansys (Ansys Inc., Pennsylvania). Ansys Mechanical was used for the structural mechanics analysis and Ansys CFX was used for the fluid mechanics computations.

2.1 Image segmentation and meshing

Patient-specific asymptomatic arterial disease ($n = 5$) and bypass graft ($n = 5$) vascular geometries were obtained from computed tomography angiography (CTA) image datasets (Ouwendijk et al. 2005). The 3D imaging software Materialise Mimics was used to manually segment the contrast-enhanced blood model using thresholding, inter-slice interpolation, region growing tools, and smoothing tools (Byrne et al. 2016). Volume and shape conserving algorithms were used. Cross-sectional areas of graft, anastomosis and artery were checked pre- and post-smoothing, and less than 2% deviation was achieved. The model was exported in STL format and further processed in Autodesk Meshmixer. Since the imaging data included all vascular structures distal to the diaphragm, the vascular model was cut to the region of interest around the distal anastomosis while maintaining minimum inflow and outflow lengths (Wang et al. 2020). The structural models were generated from the segmented fluid geometry via an offset function of 1.2 mm (Beach et al. 1989) and 0.64 mm (Lenz et al. 1998; Marin et al. 1993) for the arterial and graft segments, respectively. The latter was assumed to be representative of the thickness of both vein and ePTFE grafts. Both structural and fluid models were meshed in Ansys ICEM (Chen et al. 2021; Campobasso et al. 2018) as unstructured tetrahedral meshes with an average size of 0.3 mm (Ghaffari et al. 2017). Ten boundary fitted prism layers decreasing in size towards the wall were generated to ensure more accurate WSS data (Rabbi et al. 2020), as shown in Fig. 1. A transient mesh sensitivity analysis was performed for each patient case with regards to velocity, pressure, and wall shear stress for the fluid mesh, and deformation and von-Mises stress for the structural mesh. The mesh study was conducted on vein grafts with polypropylene sutures, since this material combination led to the highest von-Mises stresses. Results were considered mesh-independent when the difference of these parameters was less than 2% compared with a mesh with an increase of 150% in the number of nodes. Full details of the conducted sensitivity tests can be found in the supplementary materials.

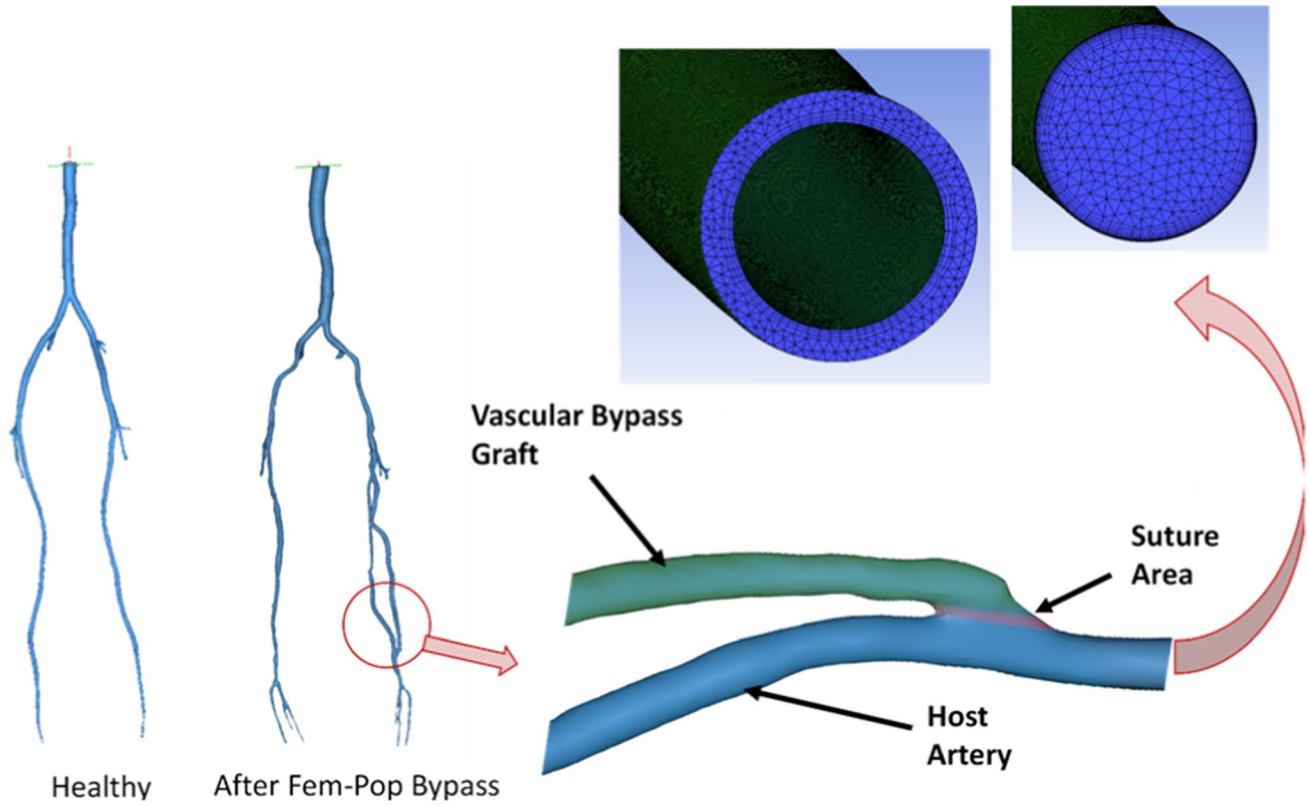

Fig. 1 Structural model generation from STL geometry to material assignment to meshing

2.2 Blood fluid model

In large and medium-sized arteries with high blood velocity magnitude and shear rates, it is common to assume that blood acts as a Newtonian fluid (Jayendiran et al. 2018b; Savabi et al. 2020; Alimohammadi et al. 2015), which can reduce model complexity. While blood flow has been accurately simulated as a Newtonian fluid in small-diameter blood vessels such as the coronary arteries (Chaichana et al. 2012; Vimmr and Jonášová 2010), these results cannot be translated to peripheral small-diameter arteries (Vimmr and Jonášová 2010) or where regions of blood stasis can occur, such as in the peripheral artery grafts here, because shear rates are significantly lower in these locations.

Previous reviews (Schoenborn et al. 2022) describe how an unsuitable choice of blood viscosity model leads to differences in WSS and velocity magnitude as high as 60% when compared with patient in vivo measurements, such as PC-MRI or Doppler US data (Abbasian et al. 2020). The non-Newtonian Carreau-Yasuda, modified Casson, or Quemada blood rheological models are frequently used to produce more accurate results in CFD simulations of blood flow dynamics (Abbasian et al. 2020). Due to its ability to capture the shear-thinning properties of blood over a wide range of shear rates, the Carreau-Yasuda model is the most commonly used non-Newtonian blood viscosity model for vascular FSI (Pinho et al. 2019; Amiri et al. 2019; Wang et al. 2021).

In this study, the Carreau-Yasuda model was used to model the blood viscosity (Rabbi et al. 2020; Boyd et al. 2007). The apparent viscosity η is given by the shear rate $\dot{\gamma}$, empirically determined constant parameters a, n, and λ, and viscosities $\eta_0 = \lim_{\dot{\gamma}\to 0}\eta(\dot{\gamma})$ and $\eta_\infty = \lim_{\dot{\gamma}\to\infty}\eta(\dot{\gamma})$

$$\eta(\dot{\gamma}) = \eta_\infty + \left(\eta_0 - \eta_\infty\right)\left[1 + (\lambda\dot{\gamma})^a\right]^{\frac{n-1}{a}} \tag{1}$$

with $\eta_\infty = 0.0035\ \text{Pa}\cdot\text{s}$, $\eta_0 = 0.1600\ \text{Pa}\cdot\text{s}$, $\lambda = 8.2\ \text{s}$, $a = 0.64$, and $n = 0.2128$ (Boyd et al. 2007).

A time-dependent velocity profile was prescribed at the inlet of the fluid model as the inflow boundary condition and a time-dependent pressure profile was prescribed at the outlet. Boundary conditions were assumed to be uniform over the cross-section of the inlet and outlet. Both the inflow and outflow velocity or pressure boundary conditions were described as eighth-order Fourier series fit:

$$p, v(t) = a_0 + \sum_{i=1}^{n}\left(a_i\cos(i\omega t) + b_i\sin(i\omega t)\right) \tag{2}$$

$$\omega = \frac{2\pi}{T} \tag{3}$$

where a_0 models a constant intercept term in the data and is associated with the $i = 0$ cosine term, ω is the fundamental frequency of the signal, T is the signal's period, i.e., the cardiac cycle length, and $n(= 8)$ is the number of terms in the series. The Fourier series were fitted to pressure and velocity data taken from the Pulse Wave Database (PWD) for a 65-year-old patient (Charlton et al. 2019). The model was fitted for two heartbeats to ensure periodicity, using the MATLAB (MathWorks, Massachusetts) Curve Fitting tool (Table S1).

A transient analysis was performed with a Second Order Backward Euler transient scheme and high resolution (2nd order iteratively bounded) advection scheme. In asymptomatic patient models, a laminar fluid model was applied with a time step size of 10^{-3} s. This was selected via a timestep sensitivity analysis. Timestep convergence was considered achieved when the change in wall shear stress, velocity, and pressure was less than 1% for a given timepoint after halving the time step size (please refer to supplementary materials). In patient models with bypass grafts, laminar simulations were compared with those using scale-resolving turbulence models such as the Stress Blended Eddy Simulation (SBES) model, which applies the *k-ω* SST model in the near-wall region and a Large Eddy Simulation model away from the wall with the transition between the two accomplished using a blending function. No turbulent flow features were found, which is in agreement with typical Reynolds numbers in peripheral arteries and the current literature (Ivanova et al. 2022). A timestep was considered as converged when the Root Mean Square (RMS) residuals of the mass conservation equation and the momentum conservation equations were all below a residual target of 10^{-4} and the mesh deformation equation was below a residual target of 10^{-5}. The model was run for two cardiac cycles after confirmation of cyclic convergence, where differences in wall shear stress, velocity, and pressure between cycle 2 and 3 were less than 0.5% for each corresponding timestep, and only the last cycle was analysed to eliminate transient start-up effects from the results.

Since flow properties change throughout the cardiac cycle, time-averaged parameters such as the time-averaged WSS magnitude (TAWSS) and time-averaged WSS vector (TAWSSV) are commonly analysed in biological flows (Piatti et al. 2017) and have become a valuable tool to predict restenosis in peripheral arteries for low TAWSS (<0.5 Pa) (Ninno et al. 2023):

$$TAWSS = \frac{1}{T}\int_0^T \left|\overrightarrow{WSS}\right| dt \tag{4}$$

$$TAWSSV = \frac{1}{T}\left|\int_0^T \overrightarrow{WSS} dt\right| \tag{5}$$

Both parameters can be combined into the oscillatory shear index (OSI), with OSI values larger than 0.15 being considered a risk factor in the development of arteriosclerosis and IH (Teng et al. 2021; Chen et al. 2017) and OSI larger than 0.2 well-applied to predict peripheral artery restenosis (Ninno et al. 2023), since it indicates large temporal variations of low and high WSS being present in recirculation zones:

$$OSI = 0.5 \times \left(1 - \frac{TAWSSV}{TAWSS}\right) \tag{6}$$

2.3 Artery structural model

A hyperelastic first-order Ogden model was utilised to reproduce the arterial wall's stress–strain behaviour (Karimi et al. 2014; Bosi et al. 2016; Schiavone and Zhao 2015). The Ogden model parameters were determined using the Ansys hyperelastic curve fitting function on circumferential uniaxial tensile testing data of healthy femoral arteries reported in the literature (Jadidi et al. 2021). The model parameters utilised for a 65-year-old patient are calculated via the Ansys Curve Fitting Tool for hyperelastic materials using published mechanical testing data on femoral arteries and are summarised in Table 1. The tissue surrounding the femoral artery was expected to have a damping effect on the arterial wall movement, which was taken into account by applying a linear elastic support boundary condition (Lantz et al. 2011). The structural model was run as a transient analysis using the sparse direct solver with a time-step size matching the fluid solver. A timestep was considered as converged when the force convergence value and the displacement convergence value were both below a residual target of 10^{-4}. The structural model was pre-stressed using a ten-step iterative pre-stress pipeline following Caimi et al. (Caimi et al. 2020), which we previously adapted for Ansys and experimentally validated in idealised small-diameter cylindrical models (Schoenborn et al. 2023).

Table 1 First-order Ogden model parameters of structural arterial wall model

Parameter	Value	Source [reference]
$\mu_{1,}$	26.414 kPa	Ansys curve fitting tool, source data from literature (Jadidi et al. 2021)
α_1	14.405	Ansys curve fitting tool, source data from literature (Jadidi et al. 2021)
d_1	3.63×10^{-6} Pa^{-1}	Literature (Schiavone and Zhao 2015)
ρ	1080 kg m^{-3}	Literature (Duck 1990)

Incompressibility parameter d_1, material constant α_1, material constant μ_1, density ρ

2.4 Graft and suture structural models

Idealised models of artery-graft anastomoses explicitly modelling the sutures are employed to accurately model the stresses and deformations at the anastomosis region for different graft-suture material combinations. The results from these idealised models were utilised to inform isotropic linearly elastic material models to model the anastomotic region in the patient-specific simulations (Fig. 1). Specifically, the isotropic linear elastic material parameters in the simplified models were calibrated to match the deformation and von-Mises stress responses of the explicitly modelled sutures in the idealised models within a 2% tolerance averaged across the stitch length. The rationale behind this approach is primarily driven by computational efficiency as the inclusion of suture contacts in full-scale 3D patient-specific FSI simulations would increase the computational cost for each patient case to impractical magnitudes. This method effectively strikes a balance between the analysis of suture line stresses without significant loss of accuracy with the possibility to study a larger number of patient models and follows similar strategies employed in other numerical patient-specific vascular models in literature, particularly in the study of stents and grafts (Menichini et al. 2018).

A continuous suture with a circular cross-section and diameter $D_{O,\,Suture} = 0.07$ mm (Suture Sizes and Suggested Indications for their use 2015) was modelled as depicted in Fig. 2. The contact between suture and artery or graft is assumed to be a frictional contact with a coefficient of friction $\mu_F = 0.43$.

The elastic modulus of the PP suture is determined by linear regression using tensile testing data published by Dobrin et al. (Dobrin 1988) and is in agreement with data published on the mechanical properties of PP elsewhere (Ineos Olefins

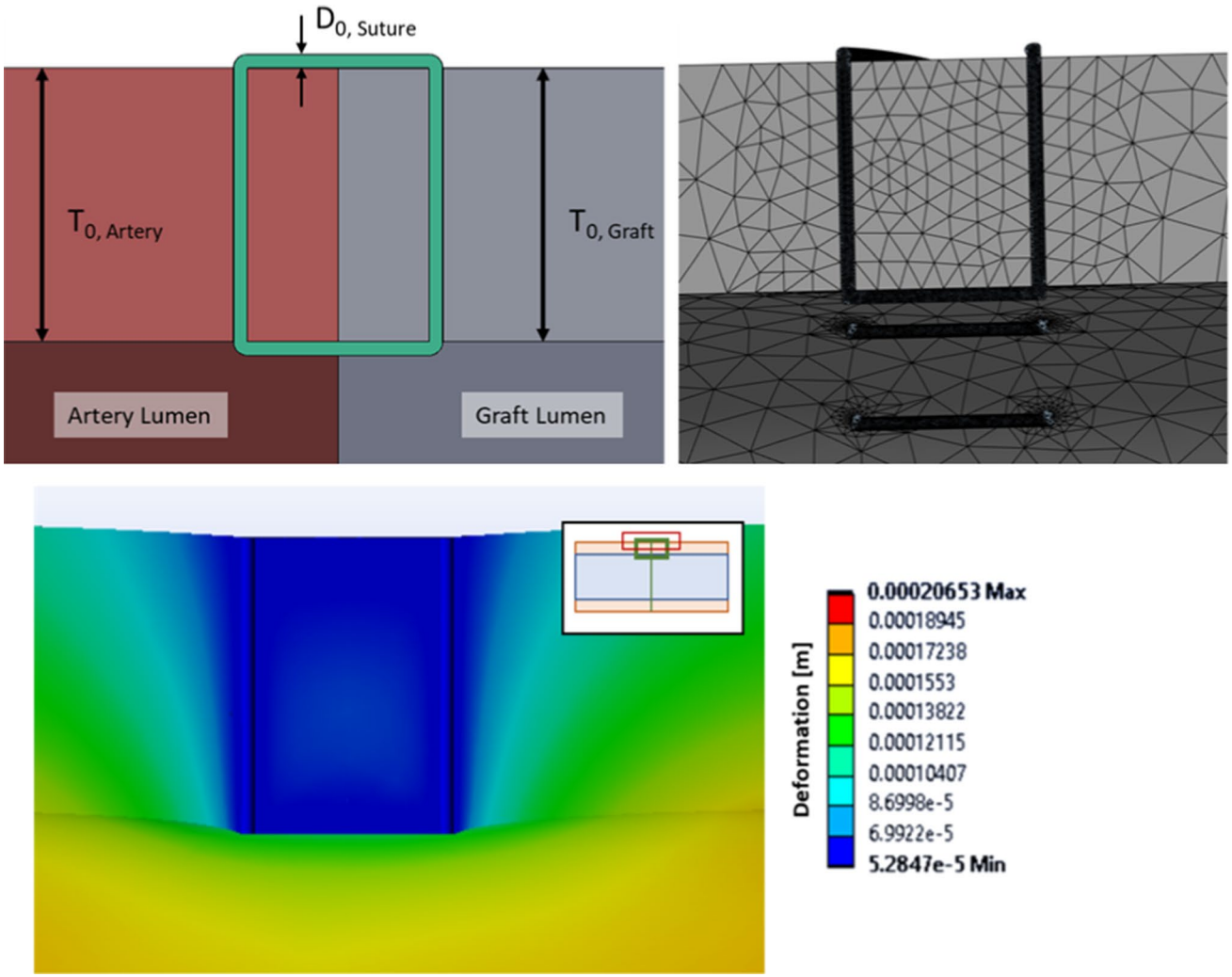

Fig. 2 Simplified geometry of a continuous polypropylene suture with a diameter $D_{O,Suture}$ in an anastomosis between an artery with thickness $T_{O,Artery}$ and graft with thickness $T_{O,Graft}$

Table 2 Properties of the polypropylene and polybutester sutures

Material	Density [kg/m^3]	Elastic modulus [MPa]	Poisson's ratio
Polypropylene	900 (Ineos Olefins Polymers et al. 2010)	1483 (Dobrin 1988; Ineos Olefins Polymers et al. 2010)	0.42 (Ineos Olefins Polymers et al. 2010)
Polybutester	1220 (Poly(4-hydroxybutyrate), Polym. xxxx)	196.2 (Martin and Williams 2003)	0.35 (Greaves et al. 2011)

Table 3 First-order Ogden model parameters of structural saphenous vein graft model

Parameter	Value	Source [reference]
$\mu_{1,}$	8.577 kPa	Ansys curve fitting tool, source data from literature (Rassoli et al. 2015)
α_1	65.221	Ansys curve fitting tool, source data from literature (Rassoli et al. 2015)
d_1	3.63×10^{-6} Pa^{-1}	Literature (Schiavone and Zhao 2015)
ρ	1080 kg m^{-3}	Literature (Duck 1990)

Incompressibility parameter d_1, material constant α_1, material constant μ_1, density ρ.

Polymers et al. 2010). The suture materials are modelled as linearly elastic as outlined in Table 2. The PP suture is compared with an alternative more compliant suture made of polybutester (PB).

Similar to the femoral arterial wall, the saphenous veinous wall shows a J-shaped nonlinear mechanical behaviour. While the saphenous vein is more compliant than the femoral artery at the low luminal pressures typically present in the venous system, it is markedly less circumferentially compliant at the high luminal pressures it is subjected to after implantation into the arterial system (Lee and Han 2010; Tai et al. 2000). This nonlinear stiffening of the veinous wall leads to a compliance mismatch with the more compliant arterial wall under arterial pressure, which is however less pronounced than the compliance mismatch between artery and synthetic graft materials, such as ePTFE (Tai et al. 2000). A first-order Ogden model was chosen to describe the behaviour of the saphenous veinous wall graft material. The model parameters utilised for saphenous vein graft are summarised in Table 3. A linear elastic material model was chosen to describe the behaviour of the ePTFE graft material (Table 4).

2.5 Fluid–structure interaction system coupling

Ansys System Coupling was used to facilitate two-way data transfers between the outer surface of the fluid volume and on the luminal surface of the structural model (Chimakurthi et al. 2018). A time step was considered converged when the individual solvers had converged and the force and displacement coupling data transfers had met an RMS convergence target of 10^{-2} (Lee et al. 2023; Shav et al. 2014). Fluid mesh deformation was calculated using a displacement diffusion model without remeshing. The flow solution was stabilised to prevent divergence by setting a velocity-dependent source coefficient in the pressure equation at the arterial wall and monitoring monotonical convergence for a given time step by plotting the forces and displacements at the arterial wall boundary (Cheng et al. 2014).

2.6 Statistical analysis

Statistically-significant differences between simulated asymptomatic and bypass graft patient anastomosis angles, percent area of high oscillatory shear index (OSI > 0.15), and percent area of high or low time-averaged wall shear stress (TAWSS > 3 Pa or TAWSS < 0.5 Pa) were calculated using p-values from Student's bidirectional t-test, assuming unpaired asymptomatic and grafted patients of equal variance. Linear correlations between anastomosis angle with percent area of high oscillatory shear index, or high, or low time-averaged wall shear stress were calculated from Spearman's R^2 coefficient, as shown in Fig. 3.

3 Results

3.1 Greater anastomotic angles enlarge 'Toe' Regions of low blood shear stress and high oscillatory blood flow

Proximal to the anastomosis, a fully developed laminar Womersley flow profile through the graft is observed with no flow in the occluded artery, with Womersley numbers of 3.6–6.4 in bypass cases and 3.9–6.8 in asymptomatic

Table 4 Properties of the ePTFE graft model

Density [kg/m^3]	Elastic modulus [MPa]	Poisson's ratio
3360 (Jorgensen and Paaske 1998)	17.4 (Bouchet et al. 2019)	0.46 (Bouchet et al. 2019)

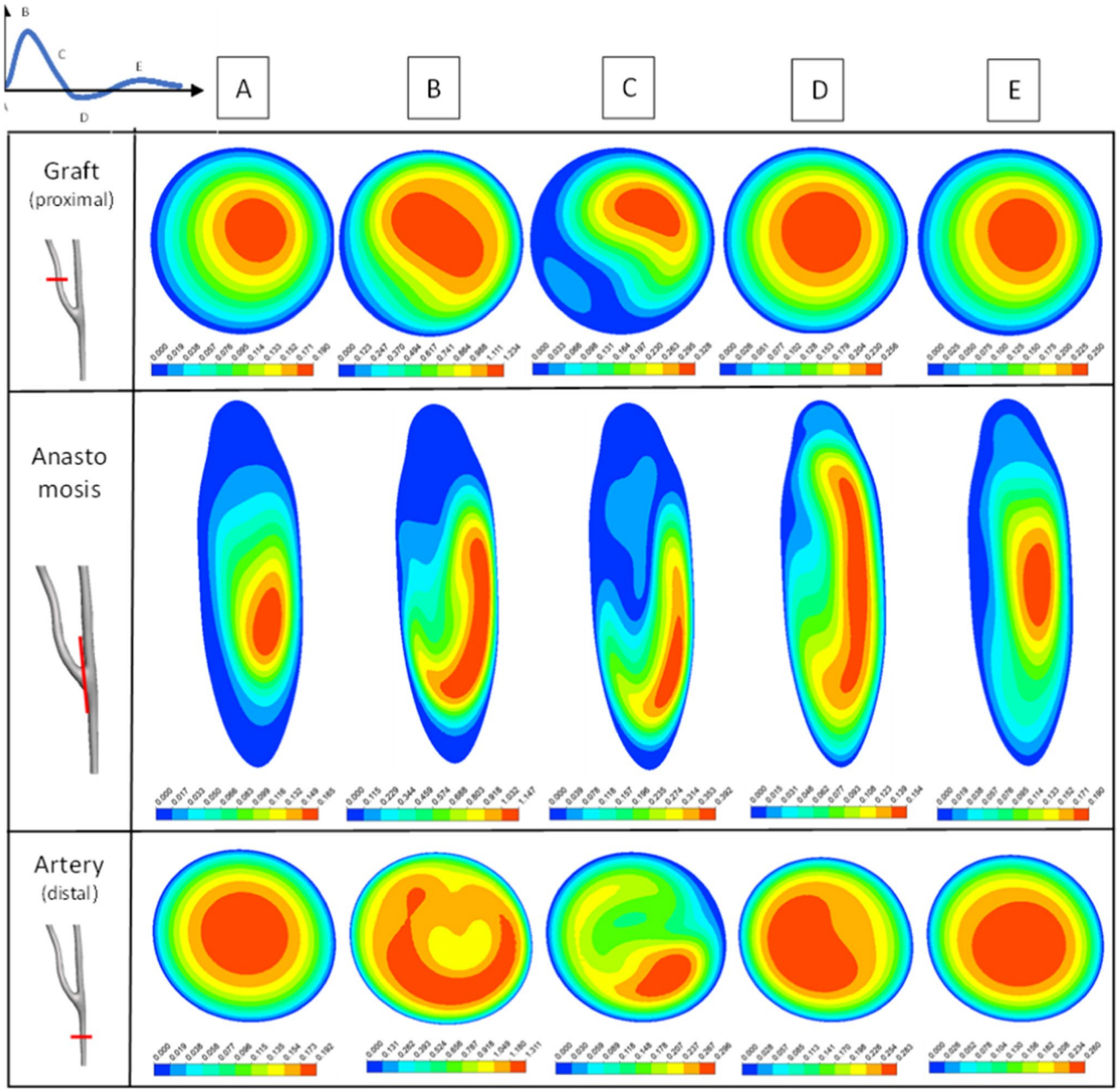

Fig. 3 Local velocity magnitude (in $m.s^{-1}$) profiles in femoral-popliteal bypass graft (top) proximal to distal anastomosis, (middle) at distal anastomosis, and (bottom) in host artery distal to distal anastomosis along cardiac cycle. Each of these three locations contains five cross-sectional velocity magnitude profiles, corresponding to five time points along a cardiac cycle (as illustrated top-left)

cases. Reynolds numbers varied from 13 to 1014 in bypass cases (average 280) versus 6–854 in asymptomatic cases (average 222), as in Supplemental Table S1. At the anastomosis, a transition to disturbed flow is observed with high velocity and WSS at the toe of the anastomosis and eddies and dead zones at the heel of the anastomosis (Fig. 4). At and distal to the anastomosis, zones of recirculation and oscillatory flow behaviour were observed in all five patient cases, resulting in 25.29–72.59% of regions within a length of 5 vertical centimetres of the anastomosis site to exhibit elevated OSI values depending on anastomosis angle (Fig. 5).

In all bypass graft patients, a recirculation zone is observed at the toe of the anastomosis, with the size of the recirculation zone being positively correlated with larger anastomosis angles ($R^2 = 0.96$, Fig. 3B) and appearing to have larger-magnitude downstream vorticity, consistent with prior experimental flow models (Grus et al. 2016). A larger,

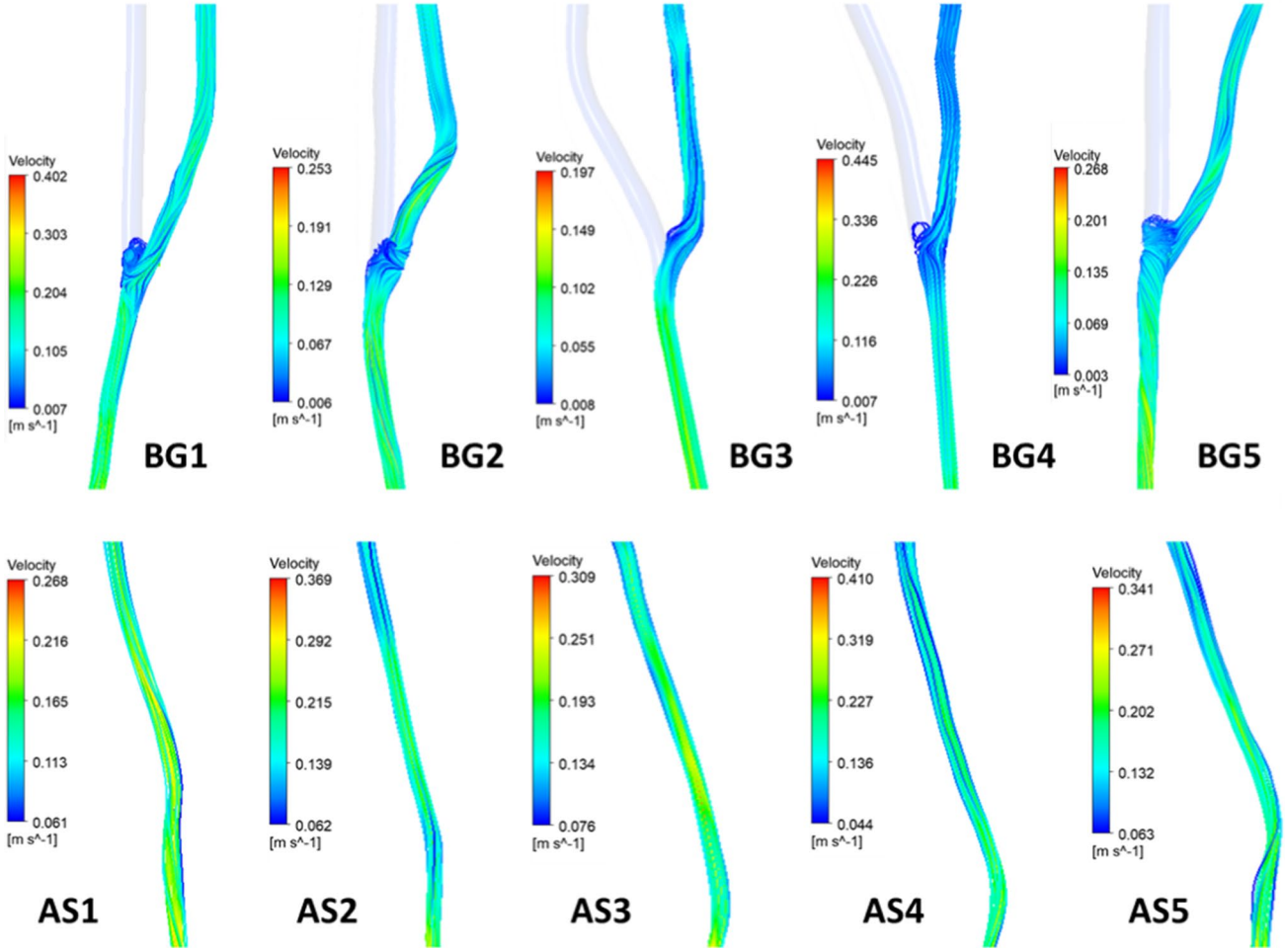

Fig. 4 Velocity streaklines at mid-diastole for five patient-specific ePTFE-PP distal femoral-popliteal bypass graft models (BG; top row) and for five patient-specific asymptomatic femoral-popliteal segment models (AS; bottom row)

i.e., more obtuse anastomosis angle as measured between the graft and host artery towards the heel of the anastomosis, is associated with a larger region of the arterial wall subjected to high OSI and low TAWSS values (TAWSS < 0.5 Pa; Fig. 3 and Table S2). Conversely, the lowest anastomosis angles were slightly correlated to have larger regions experiencing high TAWSS values (TAWSS > 3 Pa; $R^2 = 0.56$; Fig. 3C).

In the asymptomatic femoral-popliteal segments, regions of disturbed flow (OSI > 0.15) were significantly reduced compared with the grafted patient cases with $11.92\% \pm 7.81\%$ versus $50.16\% \pm 15.93\%$ ($p = 0.005$) (Fig. 3). There is no statistically significant difference in the areas of high WSS (TAWSS > 3 Pa) with $2.55\% \pm 2.00\%$ for asymptomatic vs $3.41\% \pm 5.26\%$ for grafted patient cases ($p = 0.8$) (Fig. 3). Conversely, there were no areas of low WSS (TAWSS < 0.5 Pa) in the asymptomatic geometries, vs $10.56 \pm 2.90\%$ in the grafted geometries ($p = 0.002$) as shown in Fig. 6 and Table S3.

Regions of high OSI and low TAWSS existed on and around bypass graft polypropylene sutures, representing structures of nonphysiologically low compliance and high stiffness with elevated Von Mises Stress (Fig. 7). The vascular tissue bordering the stiff sutures experienced high deformation (Fig. 8), resulting in a para-anastomotic hypercompliance zone consistent with clinical findings for femoro-popliteal artery bypass grafts (Stansby et al. 2001).

3.2 Stiffer graft and suture materials lead to larger regions of high stress and strain

The compliance of graft and suture showed small effects on tested fluid parameters for bypass graft patient BG1. For this single patient replicate, regions of elevated OSI made up 72.59, 72.46, 72.39, and 72.69% of ePTFE-PP, ePTFE-PB, Venous-PP, and Venous-PB anastomotic regions, respectively. For patient BG1, TAWSS were reduced for the more compliant saphenous vein graft material with anastomotic

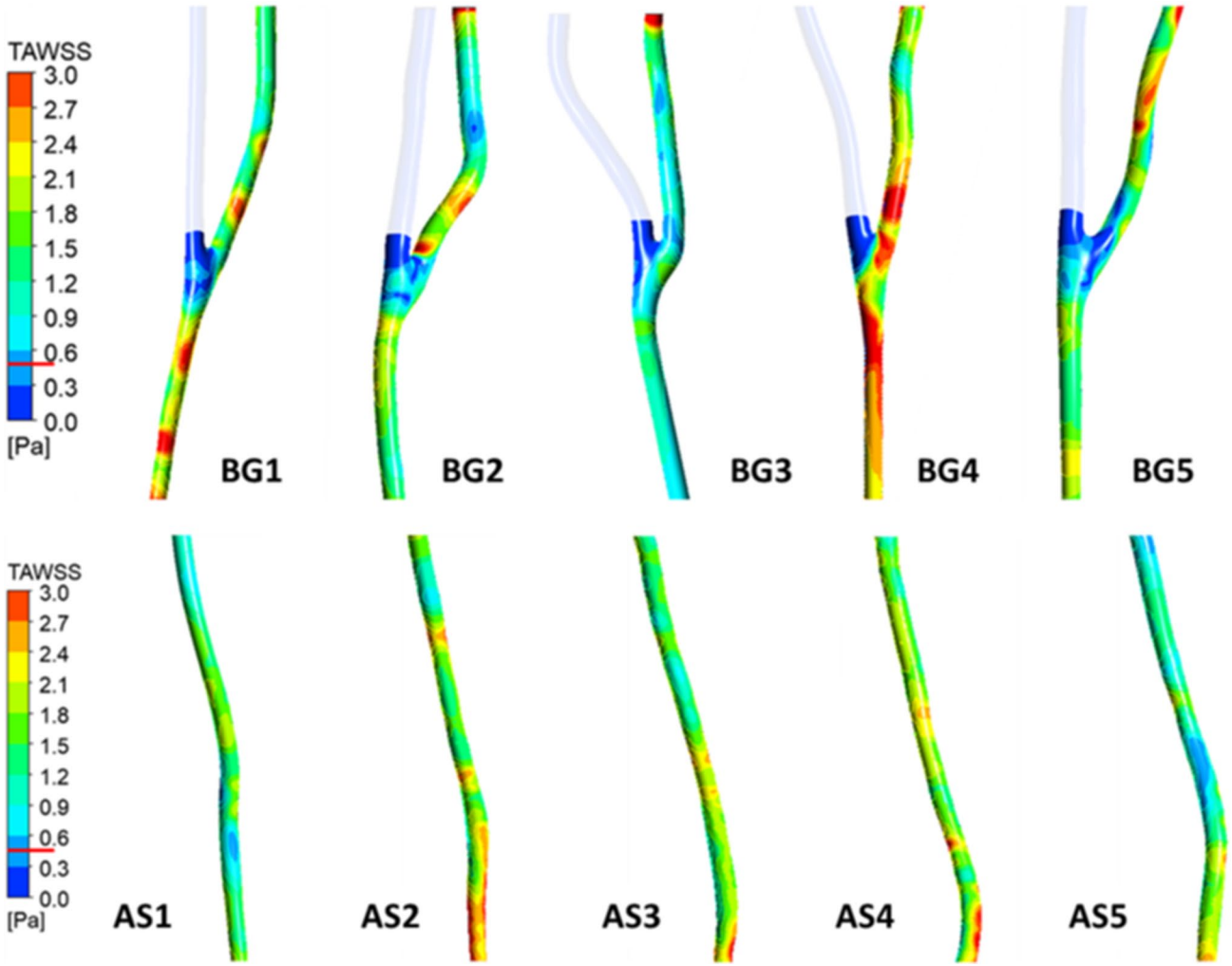

Fig. 5 Time-averaged wall shear stresses for patient-specific ePTFE-PP distal femoral-popliteal bypass graft models (BG; top row) and of patient-specific asymptomatic femoral-popliteal segment models (AS; bottom row). Red line on colorbar annotates a TAWSS of 0.5 Pa

regions being subjected to areas of 2.70, 2.73, 0.49, and 0.31% of high TAWSS and 9.06, 9.08, 9.32, and 9.39% of low TAWSS for ePTFE-PP, ePTFE-PB, Venous-PP, and Venous-PB anastomotic regions, respectively (Table 5).

In comparison with the average wall stresses of the asymptomatic patient-specific femoral-popliteal segments of 32.12 ± 4.53 kPa (AS1 to AS5), which are in good agreement with in vivo data reported in the literature (Desyatova et al. 2018), average wall stresses around patient BG1's anastomosis were elevated with 284.05, 251.21, 300.33, and 261.43 kPa for ePTFE-PP, ePTFE-PB, Venous-PP, and Venous-PB anastomoses, respectively.

The use of a more compliant suture material resulted in reduced von-Mises stress of the arterial model at patient BG1's anastomosis site (1 cm distal), while the combination of a compliant graft material with a stiff suture material resulted in the highest stresses in the arterial wall around the anastomosis (Table 5), which is associated with the proliferation and migration of VSMCs leading to IH and potential graft failure (C. M.J. et al.. 2012).

4 Discussion

Re-stenosis due to IH is one of the most common causes of mid-term vascular bypass grafts, particularly in below-the-knee applications and when for the application of synthetic graft materials. The initial trigger for the development of IH is the localised vascular trauma to the vascular wall which occurs during surgery, disrupting the endothelial and medial smooth muscle cells which in turn release various principle factors, mitogens, cytokines, and growth factors, which stimulate the quiescent vascular smooth muscle cell into a proliferative phase (Cao et al. 2022a). A range of biological,

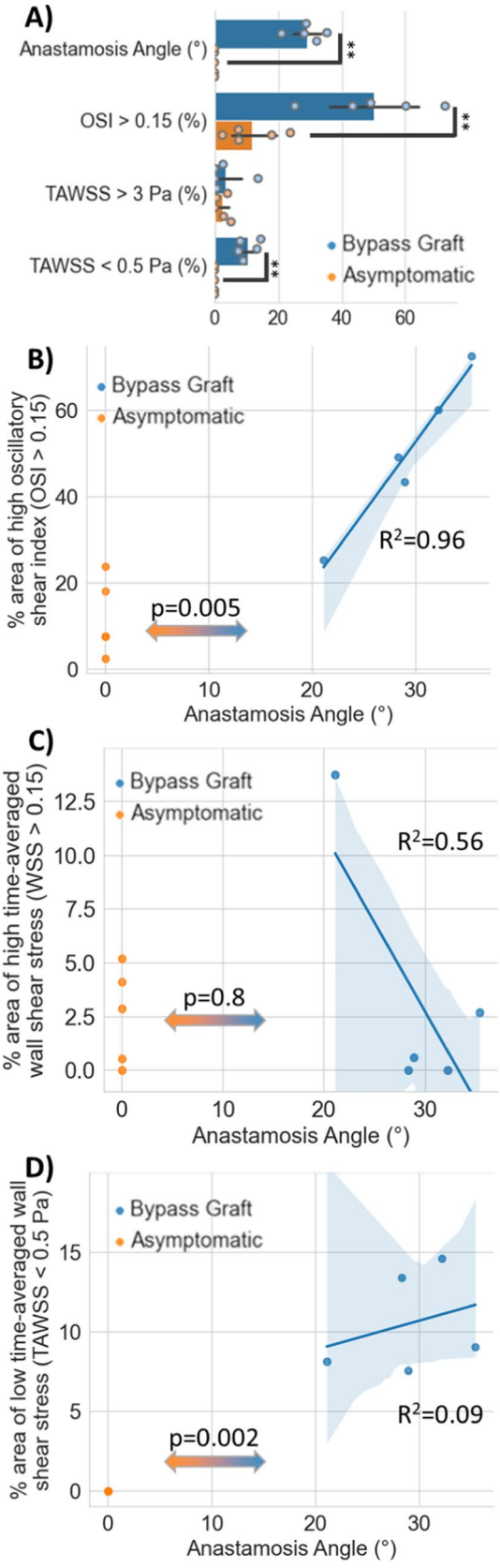

Fig. 6 Summary plots comparing simulations for ePTFE-PP grafted patients (in blue) and asymptomatic controls (in orange). Pairwise student's t-tests were preformed between asymptomatic and grafted patient scans, with p-values annotated in A and then repeated in B–D. Pearson's R^2-coefficient was applied to measure linear correlations between graft anastomosis angle and OSI or TAWSS percent. Exact values for anastamosis angle, OSI shear index, or TAWSS percentage can be found for each patient in Tables S2 and S3

chemical, and mechanical factors have been studied with regards to their potential to aggravate the severity of IH, and compliance mismatch of graft and anastomosis with the host artery is one of the central biomechanical issues of vascular graft design, as greater compliance mismatch is associated with greater incidence and severity of IH and consequently lower mid-term patency rates.

FSI simulations are an essential tool for vascular in silico studies since they can be utilised to model the fluid and structural domains of the circulatory system, along with their interaction, both for native and synthetic deformable models. FSI studies are particularly useful where changes in vascular compliance, which may occur during disease or after surgical intervention, are of interest. Biomechanical parameters which have been deemed relevant with regards to intimal hyperplasia and graft failure are wall shear stress, wall stress, and disturbed flow as characterised by high oscillatory shear index, consistent with recent peripheral artery studies (Schoenborn et al. 2022; Owida et al. 2012; Ninno et al. 2024). Relative residence time (RRT = $1/[(1 - \mathrm{OSI}) \times \mathrm{WSS}]$) is another useful metric in evaluating platelet activation or thrombosis risk in small-diameter arteries such as intracranial aneurysms (S. S.-I. et al. 2013), identifying regions containing both high OSI and low WSS. However, its definition results in a quantity with units of Pa^{-1}, which makes its interpretation difficult.

Optimising the anastomosis angle is essential to achieve favourable haemodynamic conditions. The ideal angle may vary depending on factors such as the size and type of graft, the characteristics of the native vessel, and the patient's specific condition. In vivo studies have indicated that disturbed flow patterns (high OSI) and regions of excessively low or high WSS should be avoided (Meirson et al. 2015; Keynton et al. 2001). An unfavourable graft-to-host-artery diameter ratio combined with a low (acute) anastomosis angle may lead to regions of high WSS just downstream of the anastomosis, which are associated with areas of rapid, unidirectional flow and may potentially lead to endothelial damage or remodelling (Migliavacca and Dubini 2005). On the other hand, obtuse angles may lead to regions of low WSS and high OSI near the anastomotic site, typically associated with areas of recirculation or stagnation, which may be

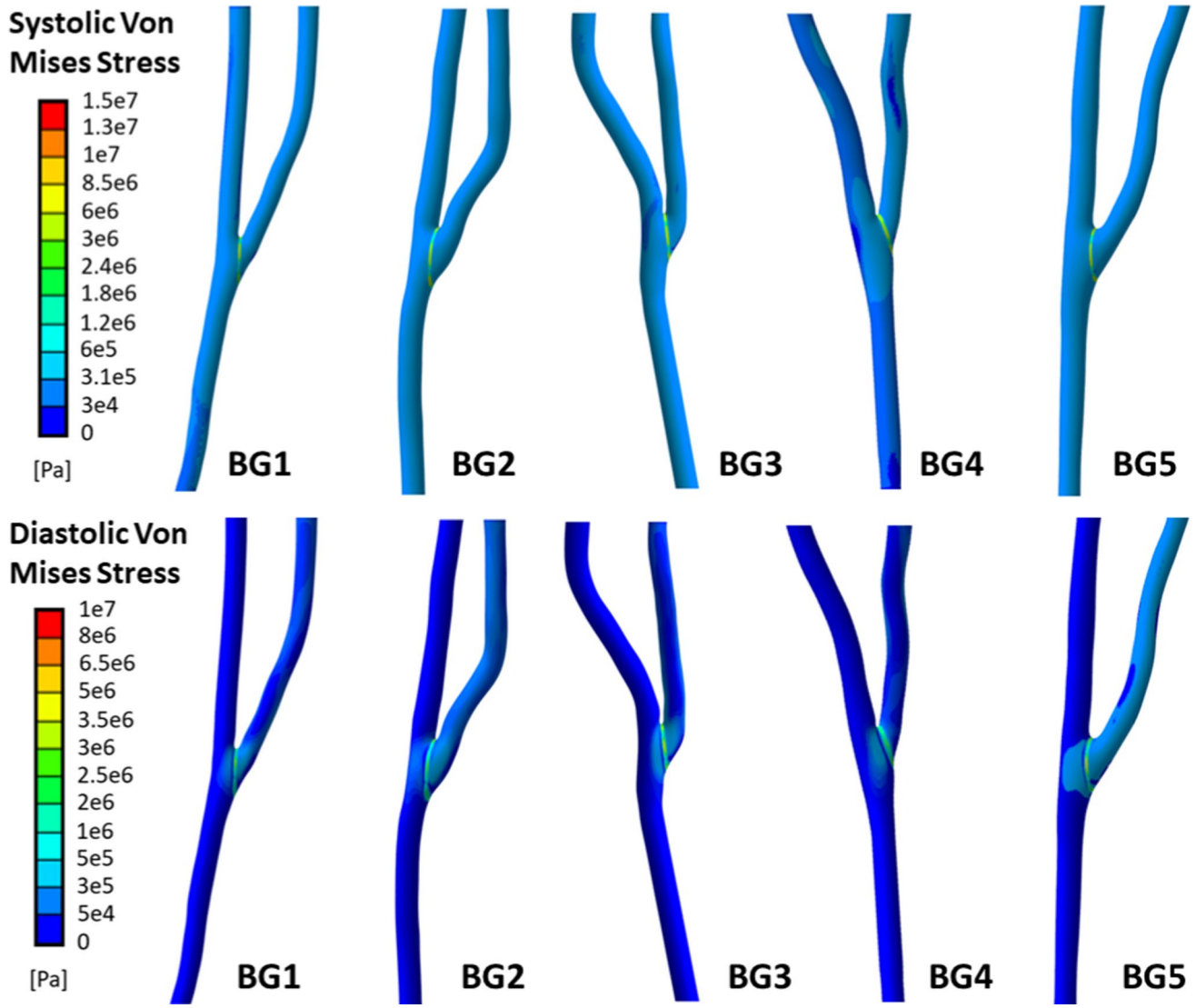

Fig. 7 Von Mises Stress heatmaps of patient-specific ePTFE-PP distal femoral-popliteal bypass graft models at systole (top row) and diastole (bottom row). A comparison of bypass grafts versus asymptomatic patient heatmaps can be found in Supplemental Figs. S1-S2

a risk factor for the development of atherosclerosis and thrombosis, as it can promote endothelial dysfunction and platelet activation (Freshwater et al. 2006). OSI is a measure of the directionality and magnitude of changes in shear stress during the cardiac cycle. OSI above zero are expected due to the pulsatility and partial backflow of blood flow across cardiac cycles. However, high OSI values indicate disturbed, oscillatory, or significantly reversing flow patterns, which are unphysiological in small-diameter arteries.

We observed regions of flow separation and recirculation indicated by low TAWSS and high OSI at the heel and toe of the anastomosis for all patient models, which is in good agreement with other studies and has been indicated as a risk factor for IH as significant lesions usually occur in this region (Sankaranarayanan et al. 2005). While this effect may be partially attributed to the geometric composition of end-to-side anastomoses, low-WSS recirculation zones have also been reported in idealised end-to-end FSI studies where blood flows from a low-compliance into a high-compliance vessel, i.e., at the distal anastomosis between a host artery and stiff graft or proximal anastomosis between a host artery and a graft with a mechanical compliance that exceeds arterial compliance (Cao et al. 2022b).

Our numerical results demonstrate non-physiological flow patterns in the anastomotic region. On the artery floor opposite the junction flow separation and zones of recirculation were found. Fluctuating WSS as indicated by a high OSI can increase the incidence and severity of IH through multiple signalling pathways, in which oxidative

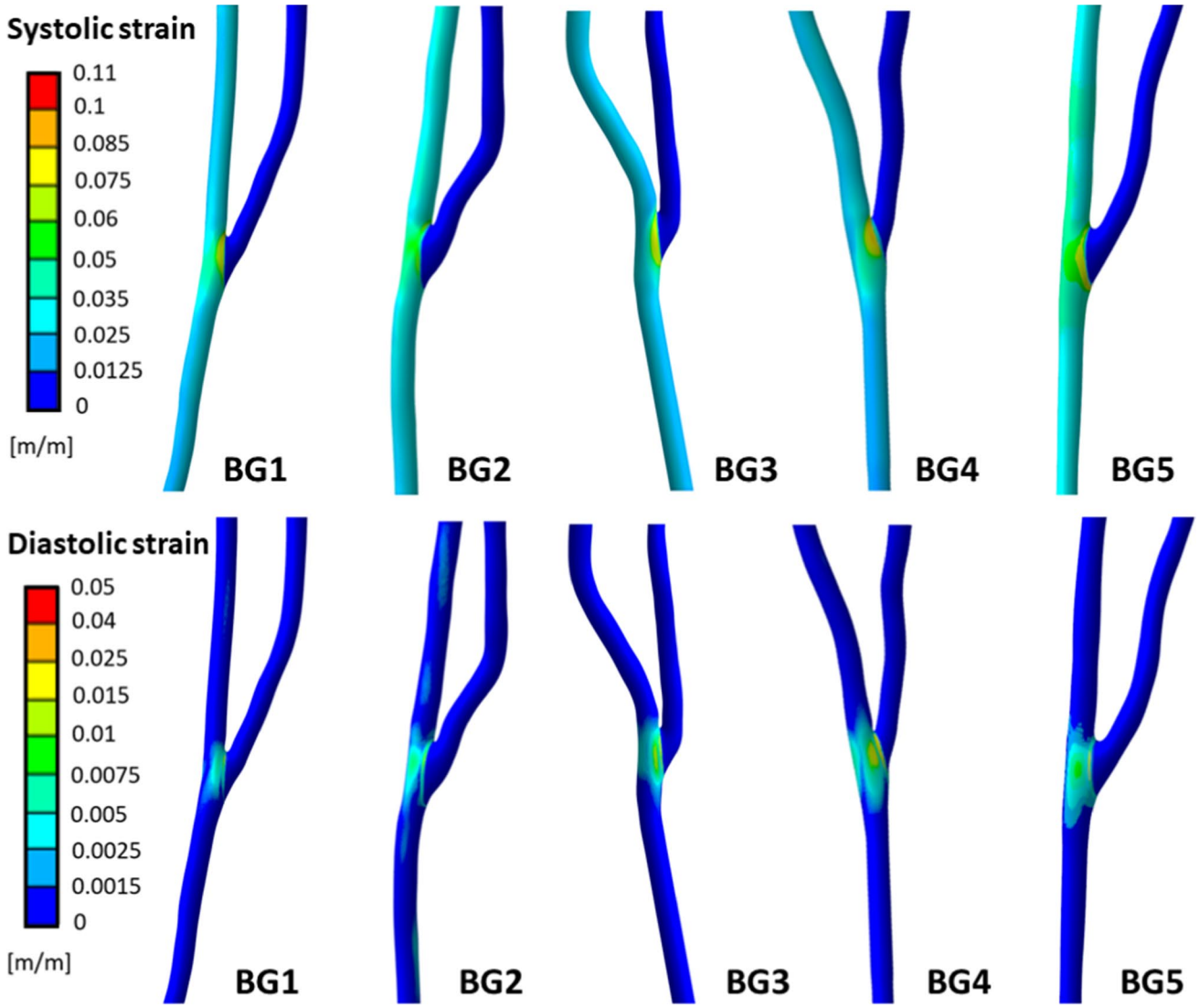

Fig. 8 Structural strain heatmaps of patient-specific ePTFE-PP distal femoral-popliteal bypass graft models at systole (top row) and diastole (bottom row). A comparison of bypass versus asymptomatic patient heatmaps can be found in Supplemental Figs. S3, S4

Table 5 Haemodynamic and structural comparison of material models for the BG1 patient case

Graft/suture material	ePTFE/PP (stiffest)	ePTFE/PB	Vein/PP	Vein/PB (compliant)
OSI > 0.15	72.59%	72.46%	72.39%	72.69%
TAWSS > 3 Pa	**2.70%**	**2.73%**	0.49%	0.31%
TAWSS < 0.5 Pa	9.06%	9.08%	9.32%	9.39%
Mean strain	4.07%	4.19%	**5.73%**	**5.97%**
Mean von-mises stress	284.05 kPa	251.21 kPa	**300.33 kPa**	261.43 kPa

Graft and suture material versus percentage of regions within anastomosis site (±5 cm) with an oscillatory shear index (OSI) above 0.15, and time-averaged wall shear stresses (TAWSS) above 3 Pa and below 0.5 Pa. Mean strain and von-Mises stress of arterial model at anastomosis site (1 cm distal). Boxes highlighted bold are above 10% of the average of their row

stress factors are implicated, promoting the proliferation, migration, and increased survival of VSMCs in the arterial intima (Yao et al. 2023). High OSI is associated with rapidly changing flow directions and high spatial and temporal WSS gradients, which may cause injury and exfoliation of the

endothelium, thus triggering the proliferation and migration of VSMCs and causing IH (Yao et al. 2023; Kim et al. 2017).

Furthermore, our results indicate an increase in graft compliance results in a decrease in adversely high TAWSS (TAWSS > 3 Pa) and a slight increase in adversely low TAWSS (< 0.5 Pa). This can be expected, as a larger vessel diameter—e.g., linked to an increased compliance—is likely to result in a lower WSS, if the cardiac output is constant. FSI models of vascular anastomoses comparing deformable and rigid vascular wall have shown that the deformation of the arterial wall has a damping effect which reduces peak wall shear stresses, but the anastomotic compliance mismatch between the arterial and graft model induces more oscillatory WSS which may contribute to the initiation of intimal hyperplasia, indicating the presence of a stiff graft within the circulatory system counteracts the protective function of the compliant arterial wall (Qiu and Tarbell 1996). However, the results of this study are limited by the lack of patient-specific boundary conditions since no clinical velocity and pressure data were available for this post-hoc analysis. Furthermore, the arterial wall and graft wall were assumed to be single-layer structures with uniform thicknesses since detailed wall models could not be extracted from the medical imaging data sets.

Our results indicate that for both PP and saphenous vein suture materials, the arterial wall movement is restricted compared with a pristine vessel, resulting in elevated stresses at the arterial wall close to the anastomosis. While the effect of the suture material on haemodynamic parameters such as WSS and OSI is minimal, the suture material compliance affects the local von-Mises stresses in the arterial wall. While the use of the more compliant PB suture material resulted in reduced von-Mises stress of the arterial model at the anastomosis site (1 cm distal), the combination of a compliant graft material with a stiff suture material resulted in the highest stresses in the arterial wall at the anastomosis. Since stress concentrations occur in connections between materials of different stiffnesses, a stiff suture material connected to two compliant graft materials leads to a stricture effect at the anastomosis with stress peaks. Conversely, optimising anastomotic compliance appears to be particularly relevant in combination with compliant grafts to minimise adverse arterial wall stresses. When compared with published in vivo animal studies on intimal hyperplasia, correlations emerge between suture line stresses and anastomotic intimal hyperplasia, with a pronounced compliance mismatch appearing to exert a proliferative effect on suture line hyperplasia (Leuprecht et al. 2002).

Our simulations remain limited in several more ways. It is important to note that our cohort of 5 bypass graft and 5 asymptomatic patient images is too small to provide clinical recommendations. Indeed, a recent review suggests 100 patients are required to begin interpreting clinical significance from small-diameter artery CFD simulation outcomes (Liu et al. 2025). Importantly, our study applies pressure and velocity boundary conditions determined for the femoral artery of a 65 year old patient from the Pulse Wave Database (Charlton et al. 2019), as flow and pressure boundary was not measured in our patients. Furthermore, in multi-branch and diseased arterial tree models, outlet impedance is known to vary significantly (Grinberg and Karniadakis 2008; Choi et al. 2025). The uniform pressure boundaries applied in this model do not capture the impact of downstream vessel diameters or resistances on flow distribution, which would potentially distort flow patterns (Du et al. 2015). Future work in adopting 3D Windkessel models (through 3D-0D coupling) or applying impedance allocation based on outlet diameters could provide a more physiologically realistic downstream vascular impedance.

5 Conclusions

This study describes a framework to simulate complex interactions between peripheral blood flow, femoropopliteal artery walls, and/or grafted material structures which are reconstructed from CTA images of five patients who have had a side-to-end bypass graft and five asymptomatic patients. Non-Newtonian fluid model and three structural models were applied to simulate the artery, the graft, and the suture material. Furthermore, all geometries were prestressed to ensure our FSI models were physiologically pressurised when simulations begun. Our patient database included graft-to-artery anastomosis angles varying between 21° and 36°, where our simulations predict that bypass grafts implanted with higher bypass anastomotic angles produce larger regions of oscillatory blood flow ($R^2 = 0.96$), especially for anastomotic angles of 28° and above. In addition, simulations of bypass graft patients contained larger zones of low vessel wall shear stress than asymptomatic patients ($p = 0.002$). Our multi-structural FSI simulation allowed us to evaluate the effect of different implant and suture materials on blood flow, where we discovered that compliant graft and suture materials are both required to reduce nonphysiologically high shear stresses downstream of the anastomosis site. Altogether, minimizing anastomosis angle and using mechanically-compliant grafts and sutures together will reduce regions of nonphysiologically low wall shear stress and high wall stresses, which are known risk factors leading to peripheral bypass intimal hyperplasia and restenosis. Our study provides a framework to simulate patient-specific fluid–structure interactions for peripheral artery grafts and presents a methodology with potential for use as a pre-surgical planning tool.

Supplementary Information The online version contains supplementary material available at https://doi.org/10.1007/s10237-025-02037-3.

Author contributions S.S. and M.C.A. concieved the project. S.S. developed and preformed all simulations and wrote the first draft of the manuscript and it's figures. T.L. and Y.S. de-identified, prepared, and supplied all clinical data and provided clinical interpretation. D.F., S.P., and M.A.W. co-supervised the project and provided computational mentorship and support. M.C.A. supervised the project, revised all later drafts of the paper for publication, and developed figures. M.C.A. and S.S. funded the project. All authors reviewed the manuscript.

Funding This work was supported by a GOstralia!-GOzealand! GmbH Scholarship to SS, a Bionics Queensland Grand Challenge Award to SS and MCA, a Delft Technology Fellowship to SP, an Advance Queensland Fellowship to MCA (AQIRF1312018), and an Australian Research Council DECRA Fellowship to MCA (DE220100757).

Data availability Data is provided within the manuscript or supplementary information files.

Declarations

Conflict of interests DFF consults to the local Ansys distributors which gives him access to Ansys technical staff as needed. The remaining authors declare that they have no known conflict of financial interests or personal relationships that could have appeared to influence the work reported in this paper.

Ethical approval Non-identifiable patient images were provided under human research ethics approval LNR/2019/QRBW/53686 and site-specific approval SSA/QMS/53686 "Vascular model biofabrication for surgical planning, training, and treatment."

References

Abbasian M, Shams M, Valizadeh Z, Moshfegh A, Javadzadegan A, Cheng S (2020) Effects of different non-Newtonian models on unsteady blood flow hemodynamics in patient-specific arterial models with in-vivo validation. Comput Methods Programs Biomed. https://doi.org/10.1016/j.cmpb.2019.105185

Alimohammadi M, Sherwood JM, Karimpour M, Agu O, Balabani S, Díaz-Zuccarini V (2015) Aortic dissection simulation models for clinical support: fluid-structure interaction vs. rigid wall models. Biomed Eng Online. https://doi.org/10.1186/s12938-015-0032-6

Amiri MH, Keshavarzi A, Karimipour A, Bahiraei M, Goodarzi M, Esfahani JA (2019) A 3-D numerical simulation of non-Newtonian blood flow through femoral artery bifurcation with a moderate arteriosclerosis: investigating Newtonian/non-Newtonian flow and its effects on elastic vessel walls. Heat Mass Transfer 55:2037–2047. https://doi.org/10.1007/s00231-019-02583-4

Aronow WS (2007) Peripheral arterial disease in the elderly. Clin Interv Aging 2:645–654. https://doi.org/10.1161/01.atv.18.2.185

Bauersachs R, Zeymer U, Brière JB, Marre C, Bowrin K, Huelsebeck M (2019) Burden of coronary artery disease and peripheral artery disease: a literature review. Cardiovasc Ther. https://doi.org/10.1155/2019/8295054

Beach KW, Isaac CA, Phillips DJ, Strandness DE (1989) An ultrasonic measurement of superficial femoral artery wall thickness. Ultrasound Med Biol 15:723–728. https://doi.org/10.1016/0301-5629(89)90112-9

Bosi GM, Biffi B, Biglino G, Lintas V, Jones R, Tzamtzis S, Burriesci G, Migliavacca F, Khambadkone S, Taylor AM, Schievano S (2016) Can finite element models of ballooning procedures yield mechanical response of the cardiovascular site to overexpansion? J Biomech 49:2778–2784. https://doi.org/10.1016/j.jbiomech.2016.06.021

Bouchet M, Gauthier M, Maire M, Ajji A, Lerouge S (2019) Towards compliant small-diameter vascular grafts: predictive analytical model and experiments. Mater Sci Eng C 100:715–723. https://doi.org/10.1016/j.msec.2019.03.023

Boyd J, Buick JM, Green S (2007) Analysis of the Casson and Carreau-Yasuda non-Newtonian blood models in steady and oscillatory flows using the lattice Boltzmann method. Phys Fluids. https://doi.org/10.1063/1.2772250

Bozzetto M, Ene-Iordache B, Remuzzi A (2016) Transitional flow in the venous side of patient-specific arteriovenous fistulae for hemodialysis. Ann Biomed Eng 44:2388–2401. https://doi.org/10.1007/s10439-015-1525-y

Bradbury AW, Moakes CA, Popplewell M, Meecham L, Bate GR, Kelly L, Chetter I, Diamantopoulos A, Ganeshan A, Hall J, Hobbs S, Houlind K, Jarrett H, Lockyer S, Malmstedt J, Patel JV, Patel S, Rashid ST, Saratzis A, Slinn G, Scott DJA, Zayed H, Deeks JJ (2023) A vein bypass first versus a best endovascular treatment first revascularisation strategy for patients with chronic limb threatening ischaemia who required an infrapopliteal, with or without an additional more proximal infrainguinal revascularisation pr. Lancet 401:1798–1809. https://doi.org/10.1016/S0140-6736(23)00462-2

Bregy A, Bogni S, Bernau VJP, Vajtai I, Vollbach F, Petri-Fink A, Constantinescu M, Hofmann H, Frenz M, Reinert M (2008) Solder doped polycaprolactone scaffold enables reproducible laser tissue soldering. Lasers Surg Med 40:716–725. https://doi.org/10.1002/lsm.20710

Brody JI, Pickering NJ (1989) Pathobiology of intimal hyperplasia. J Vasc Surg 10:583–585. https://doi.org/10.1016/0741-5214(89)90153-5

Byrne N, Velasco Forte M, Tandon A, Valverde I, Hussain T (2016) A systematic review of image segmentation methodology, used in the additive manufacture of patient-specific 3D printed models of the cardiovascular system. JRSM Cardiovasc Dis 5:204800401664546. https://doi.org/10.1177/2048004016645467

Caimi A, Pasquali M, Sturla F, Pluchinotta FR, Giugno L, Carminati M, Redaelli A, Votta E (2020) Prediction of post-stenting biomechanics in coarcted aortas: a pilot finite element study. J Biomech. https://doi.org/10.1016/j.jbiomech.2020.109796

Campobasso R, Condemi F, Viallon M, Croisille P, Campisi S, Avril S (2018) Evaluation of peak wall stress in an Ascending Thoracic Aortic Aneurysm using FSI simulations: effects of Aortic stiffness and Peripheral resistance. Cardiovasc Eng Technol 9:707–722. https://doi.org/10.1007/s13239-018-00385-z

Cao G, Xuan X, Hu J, Zhang R, Jin H, Dong H (2022a) How vascular smooth muscle cell phenotype switching contributes to vascular disease. Cell Commun Signal. https://doi.org/10.1186/s12964-022-00993-2

Cao T, Jiang Z, Zhao H, Zhang KQ, Meng K (2022b) Numerical simulation to study the impact of compliance mismatch between artificial and host blood vessel on hemodynamics. Med Novel Technol Devices. https://doi.org/10.1016/j.medntd.2022.100152

Carrabba M, Madeddu P (2018) Current strategies for the manufacture of small size tissue engineering vascular grafts. Front Bioeng Biotechnol 6:1–12. https://doi.org/10.3389/fbioe.2018.00041

Chaichana T, Sun Z, Jewkes J (2012) Computational fluid dynamics analysis of the effect of plaques in the left coronary artery. Comput Math Methods Med. https://doi.org/10.1155/2012/504367

Charlton PH, Harana JM, Vennin S, Li Y, Chowienczyk P, Alastruey J (2019) Modeling arterial pulse waves in healthy aging: a database

for in silico evaluation of hemodynamics and pulse wave indexes. Am J Physiol Heart Circ Physiol 317:H1062–H1085. https://doi.org/10.1152/AJPHEART.00218.2019

Chen Z, Yu H, Shi Y, Zhu M, Wang Y, Hu X, Zhang Y, Chang Y, Xu M, Gao W (2017) Vascular remodelling relates to an elevated oscillatory shear index and relative residence time in spontaneously hypertensive rats. Sci Rep. https://doi.org/10.1038/s41598-017-01906-x

Chen X, Zhuang J, Huang H, Wu Y (2021) Fluid–structure interactions (FSI) based study of low-density lipoproteins (LDL) uptake in the left coronary artery. Sci Rep. https://doi.org/10.1038/s41598-021-84155-3

Cheng S, Fletcher D, Hemley S, Stoodley M, Bilston L (2014) Effects of fluid structure interaction in a three dimensional model of the spinal subarachnoid space. J Biomech 47:2826–2830. https://doi.org/10.1016/j.jbiomech.2014.04.027

Chimakurthi SK, Reuss S, Tooley M, Scampoli S (2018) ANSYS workbench system coupling: a state-of-the-art computational framework for analyzing multiphysics problems. Eng Comput 34:385–411. https://doi.org/10.1007/s00366-017-0548-4

Cho KC, Yang H, Kim JJ, Oh JH, Kim YB (2020) Prediction of rupture risk in cerebral aneurysms by comparing clinical cases with fluid–structure interaction analyses. Sci Rep 10:1–8. https://doi.org/10.1038/s41598-020-75362-5

Choi JH, Cha M, Shin SM, Kim J, Kim HG, Kim BJ, Jo HJ (2025) Maximum admittance method for cerebrovascular outlet boundary conditions and importance of stenosis severity as a dominant factor on hemodynamics. Sci Rep. https://doi.org/10.1038/s41598-025-90604-0

Colley E, Carroll J, Anne S, Shannon T, Ramon V, Tracie B (2022) A longitudinal study of the arterio-venous fistula maturation of a single patient over 15 weeks. Biomech Model Mechanobiol 21:1217–1232. https://doi.org/10.1007/s10237-022-01586-1

Collins MJ, Li X, Lv W, Yang C, Protack CD, Muto ADardik A (2012) Therapeutic strategies to combat neointimal hyperplasia in vascular grafts. Expert Rev Cardiovasc Ther 10(5):635–647. https://doi.org/10.1586/erc.12.33

Conte SM, Vale PR (2018) Peripheral arterial disease. Heart Lung Circ 27:427–432. https://doi.org/10.1016/j.hlc.2017.10.014

Conte MS, Mann MJ, Simosa HF, Rhynhart KK, Mulligan RC (2002) Genetic interventions for vein bypass graft disease: a review. J Vasc Surg 36:1040–1052. https://doi.org/10.1067/mva.2002.129112

D.N. G, F. K (2013) Coronary artery bypass grafting hemodynamics and anastomosis design: a biomedical engineering review. Biomed Eng Online 12:1–29

Decorato I, Kharboutly Z, Legallais C, Salsac AV (2011) Numerical study of the influence of wall compliance on the haemodynamics in a patient-specific arteriovenous fistula. Comput Methods Biomech Biomed Engin 14:121–123. https://doi.org/10.1080/10255842.2011.593762

Decorato I, Kharboutly Z, Vassallo T, Penrose J, Legallais C, Salsac AV (2014) Numerical simulation of the fluid structure interactions in a compliant patient-specific arteriovenous fistula. Int J Numer Methods Biomed Eng 30:143–159. https://doi.org/10.1002/cnm.2595

Desyatova A, Poulson W, MacTaggart J, Maleckis K, Kamenskiy A (2018) Cross-sectional pinching in human femoropopliteal arteries due to limb flexion, and stent design optimization for maximum cross-sectional opening and minimum intramural stresses. J R Soc Interface. https://doi.org/10.1098/rsif.2018.0475

Dobrin PB (1988) Some mechanical properties of polypropylene sutures: relationship to the use of polypropylene in vascular surgery. J Surg Res 45:568–573. https://doi.org/10.1016/0022-4804(88)90146-1

Du T, Hu D, Cai D (2015) Outflow boundary conditions for blood flow in arterial trees. PLoS ONE. https://doi.org/10.1371/journal.pone.0128597

Duck FA (1990) Physical properties of tissue: a comprehensive reference book. Academic Press, London

Farber A, Menard MT, Conte MS, Kaufman JA, Powell RJ, Choudhry NK, Hamza TH, Assmann SF, Creager MA, Cziraky MJ, Dake MD, Jaff MR, Reid D, Siami FS, Sopko G, White CJ, van Over M, Strong MB, Villarreal MF, McKean M, Azene E, Azarbal A, Barleben A, Chew DK, Clavijo LC, Douville Y, Findeiss L, Garg N, Gasper W, Giles KA, Goodney PP, Hawkins BM, Herman CR, Kalish JA, Koopmann MC, Laskowski IA, Mena-Hurtado C, Motaganahalli R, Rowe VL, Schanzer A, Schneider PA, Siracuse JJ, Venermo M, Rosenfield K (2022) Surgery or Endovascular therapy for chronic limb-threatening ischemia. N Engl J Med 387:2305–2316. https://doi.org/10.1056/nejmoa2207899

Freshwater IJ, Morsi YS, Lai T (2006) The effect of angle on wall shear stresses in a LIMA to LAD anastomosis: numerical modelling of pulsatile flow. Proc Inst Mech Eng 220:743–757. https://doi.org/10.1243/09544119JEIM126

Georgakarakos E, Xenakis A, Georgiadis GS (2017) Estimating the hemodynamic influence of variable main body-to-iliac limb length ratios in aortic endografts. Int Angiol A J Int Union Angiol 37(1):41–45. https://doi.org/10.23736/S0392-9590.17.03883-4

Ghaffari M, Tangen K, Alaraj A, Du X, Charbel FT, Linninger AA (2017) Large-scale subject-specific cerebral arterial tree modeling using automated parametric mesh generation for blood flow simulation. Comput Biol Med 91:353–365. https://doi.org/10.1016/j.compbiomed.2017.10.028

Graham LM, Bassiouny HS, White SS, Glagov SS, Choi ES, Giddens DP (1992) Anastomotic intimal hyperplasia: mechanical injury or flow induced. J Vasc Surg 15:0708–0717. https://doi.org/10.1067/mva.1992.33849

Greaves GN, Greer AL, Lakes RS, Rouxel T (2011) Poisson's ratio and modern materials. Nat Mater 10:823–837. https://doi.org/10.1038/nmat3134

Grinberg L, Karniadakis GE (2008) Outflow boundary conditions for arterial networks with multiple outlets. Ann Biomed Eng 36:1496–1514. https://doi.org/10.1007/s10439-008-9527-7

Grus T, Lambert L, Matěcha J, Grusová G, Špaček M, Mlček M (2016) The ratio of diameters between the target artery and the bypass modifies hemodynamic parameters related to intimal hyperplasia in the distal end-to-side anastomosis. Physiol Res 65:901–908. https://doi.org/10.33549/physiolres.933297

Ineos Olefins & Polymers USA (2010) Typical Engineering Properties of Polypropylene, Ineos Olefin. Polym. USA. 2. http://www.ineos.com/globalassets/ineos-group/businesses/ineos-olefins-and-polymers-usa/products/technical-information--patents/ineos-engineering-properties-of-pp.pdf

Ivanova Y, Yukhnev A, Tikhomolova L, Smirnov E, Vrabiy A, Suprunovich A, Morozov A, Khubulava G, Vavilov V (2022) Experience of patient-specific CFD simulation of blood flow in proximal anastomosis for femoral-popliteal bypass. Fluids. https://doi.org/10.3390/fluids7100314

Jadidi M, Razian SA, Habibnezhad M, Anttila E, Kamenskiy A (2021) Mechanical, structural, and physiologic differences in human elastic and muscular arteries of different ages: comparison of the descending thoracic aorta to the superficial femoral artery. Acta Biomater 119:268–283. https://doi.org/10.1016/j.actbio.2020.10.035

Jayendiran R, Nour B, Ruimi A (2018a) Fluid-structure interaction (FSI) analysis of stent-graft for aortic endovascular aneurysm repair (EVAR): material and structural considerations. J Mech Behav Biomed Mater 87:95–110. https://doi.org/10.1016/j.jmbbm.2018.07.020

Jayendiran R, Nour B, Ruimi A (2018b) Computational fluid–structure interaction analysis of blood flow on patient-specific reconstructed aortic anatomy and aneurysm treatment with Dacron graft. J Fluids Struct 81:693–711. https://doi.org/10.1016/j.jfluidstructs.2018.06.008

Jeong Y, Yao Y, Yim EKF (2020) Current understanding of intimal hyperplasia and effect of compliance in synthetic small diameter vascular grafts. Biomater Sci 8:4383–4395. https://doi.org/10.1039/d0bm00226g

Jia L, Wang L, Wei F, Yu H, Dong H, Wang B, Lu Z, Sun G, Chen H, Meng J, Li B, Zhang R, Bi X, Wang Z, Pang H, Jiang A (2015) Effects of wall shear stress in venous neointimal hyperplasia of arteriovenous fistulae. Nephrology 20:335–342. https://doi.org/10.1111/nep.12394

Jodko D, Barber T (2024) Fluid–structure interaction in a follow-up study of arterio-venous fistula maturation. Sci Rep 14:1–20. https://doi.org/10.1038/s41598-024-80916-y

Jorgensen CS, Paaske WP (1998) Physical and mechanical properties of ePTFE stretch vascular grafts determined by time-resolved scanning acoustic microscopy. Eur J Vasc Endovasc Surg 15:416–422. https://doi.org/10.1016/S1078-5884(98)80203-7

Karimi A, Navidbakhsh M, Alizadeh M, Shojaei A (2014) A comparative study on the mechanical properties of the umbilical vein and umbilical artery under uniaxial loading. Artery Res 8:51–56. https://doi.org/10.1016/j.artres.2014.02.001

Kasapis C, Gurm HS (2010) Current approach to the diagnosis and treatment of femoral-popliteal arterial disease. A systematic review. Curr Cardiol Rev 5:296–311. https://doi.org/10.2174/157340309789317823

Keynton RS, Evancho MM, Sims RL, Rodway NV, Gobin A, Rittgers SE (2001) Intimal hyperplasia and wall shear in arterial bypass graft distal anastomoses: an in vivo model study. J Biomech Eng 123:464–473. https://doi.org/10.1115/1.1389461

Kim YM, Kim SJ, Tatsunami R, Yamamura H, Fukai T, Fukai MU (2017) ROS-induced ROS release orchestrated by Nox4, Nox2, and mitochondria in VEGF signaling and angiogenesis. Am J Physiol Cell Physiol 312:C749–C764. https://doi.org/10.1152/ajpcell.00346.2016

Klinkert P, Schepers A, Burger DHC, Van Bockel JH, Breslau PJ (2003) Vein versus polytetrafluoroethylene in above-knee femoropopliteal bypass grafting: five-year results of a randomized controlled trial. J Vasc Surg 37:149–155. https://doi.org/10.1067/mva.2002.86

Klinkert P, Post PN, Breslau PJ, van Bockel JH (2004) Saphenous vein versus PTFE for above-knee femoropopliteal bypass. A review of the literature. Eur J Vasc Endovasc Surg 27:357–362. https://doi.org/10.1016/j.ejvs.2003.12.027

Lantz J, Renner J, Karlsson M (2011) Wall shear stress in a subject specific human aorta - influence of fluid-structure interaction. Int J Appl Mech 3:759–778. https://doi.org/10.1142/S1758825111001226

Lee AY, Han HC (2010) A nonlinear thin-wall model for vein buckling. Cardiovasc Eng Technol 1:282–289. https://doi.org/10.1007/s13239-010-0024-4

Lee GH, Heo W, Lee Y, Kim TH, Huh H, Song SW, Ha H (2023) Fluid–structure interaction simulation of visceral perfusion and impact of different cannulation methods on aortic dissection. Sci Rep. https://doi.org/10.1038/s41598-023-27855-2

Lemson MS, Tordoir JHM, Daemen MJAP, Kitslaar PJEHM (2000) Intimal hyperplasia in vascular grafts. Eur J Vasc Endovasc Surg 19:336–350. https://doi.org/10.1053/ejvs.1999.1040

Lenz BJ, Veldenz HC, Dennis JW, Khansarinia S, Atteberry LR, Goldman MH (1998) A three-year follow-up on standard versus thin wall ePTFE grafts for hemodialysis. J Vasc Surg 28:464–470. https://doi.org/10.1016/S0741-5214(98)70132-6

Lepäntalo MJA, Houbballah R, Raux M, Lamuraglia G (2012) Lower extremity bypass vs endovascular therapy for young patients with symptomatic peripheral arterial disease. J Vasc Surg 56:545–554. https://doi.org/10.1016/j.jvs.2012.06.053

Leuprecht A, Perktold K, Prosi M, Berk T, Trubel W, Schima H (2002) Numerical study of hemodynamics and wall mechanics in distal end-to-side anastomoses of bypass grafts. J Biomech 35:225–236. https://doi.org/10.1016/S0021-9290(01)00194-4

Liu Y, Li S, Liu H, Tian X, Liu Y, Li Z, Leung TW, Leng X (2025) Clinical implications of haemodynamics in symptomatic intracranial atherosclerotic stenosis by computational fluid dynamics modelling: a systematic review. Stroke Vasc Neurol 10:16–24. https://doi.org/10.1136/svn-2024-003202

Lopes D, Puga H, Teixeira JC, Teixeira SF (2019) Influence of arterial mechanical properties on carotid blood flow: comparison of CFD and FSI studies. Int J Mech Sci 160:209–218. https://doi.org/10.1016/j.ijmecsci.2019.06.029

Mahoney EM, Wang K, Keo HH, Duval S, Smolderen KG, Cohen DJ, Steg G, Bhatt DL, Hirsch AT (2010) Vascular hospitalization rates and costs in patients with peripheral artery disease in the United States. Circ Cardiovasc Qual Outcomes 3:642–651. https://doi.org/10.1161/CIRCOUTCOMES.109.930735

Marin ML, Veith FJ, Panetta TF, Gordon RE, Wengerter KR, Suggs WD, Sanchez L, Parides MK (1993) Saphenous vein biopsy: a predictor of vein graft failure. J Vasc Surg 18:407–415. https://doi.org/10.1016/0741-5214(93)90258-N

Martin DP, Williams SF (2003) Medical applications of poly-4-hydroxybutyrate: a strong flexible absorbable biomaterial. Biochem Eng J 16:97–105. https://doi.org/10.1016/S1369-703X(03)00040-8

Mathers CD, Loncar D (2006) Projections of global mortality and burden of disease from 2002 to 2030. PLoS Med. https://doi.org/10.1371/journal.pmed.0030442

McGah PM, Leotta DF, Beach KW, Aliseda A (2014) Effects of wall distensibility in hemodynamic simulations of an arteriovenous fistula. Biomech Model Mechanobiol 13:679–695. https://doi.org/10.1007/s10237-013-0527-7

Meirson T, Orion E, Di Mario C, Webb C, Patel N, Channon KM, Ben Gal Y, Taggart DP (2015) Flow patterns in externally stented saphenous vein grafts and development of intimal hyperplasia. J Thorac Cardiovasc Surg 150:871–879. https://doi.org/10.1016/j.jtcvs.2015.04.061

Menichini C, Pirola S, Guo B, Fu W, Dong Z, Xu XY (2018) High wall stress may predict the formation of stent-graft–induced new entries after thoracic endovascular aortic repair. J Endovasc Ther 25:571–577. https://doi.org/10.1177/1526602818791827

Meyerson SL, Skelly CL, Curi MA, Shakur UM, Vosicky JE, Glagov S, Schwartz LB (2001) The effects of extremely low shear stress on cellular proliferation and neointimal thickening in the failing bypass graft. J Vasc Surg 34:90–97. https://doi.org/10.1067/mva.2001.114819

Migliavacca F, Dubini G (2005) Computational modeling of vascular anastomoses. Biomech Model Mechanobiol 3:235–250. https://doi.org/10.1007/s10237-005-0070-2

Ngoepe MN, Reddy BD, Kahn D, Meyer C, Zilla P, Franz T (2011) A numerical tool for the coupled mechanical assessment of anastomoses of PTFE arterio-venous access grafts. Cardiovasc Eng Technol 2:160–172. https://doi.org/10.1007/s13239-011-0045-7

Ninno F, Tsui J, Balabani S, Díaz-Zuccarini V (2023) A systematic review of clinical and biomechanical engineering perspectives on the prediction of restenosis in coronary and peripheral arteries. JVS-Vasc Sci 4:100128. https://doi.org/10.1016/j.jvssci.2023.100128

Ninno F, Chiastra C, Colombo M, Dardik A, Strosberg D, Aboian E, Tsui J, Bartlett M, Balabani S, Díaz-Zuccarini V (2024)

Modelling lower-limb peripheral arterial disease using clinically available datasets: impact of inflow boundary conditions on hemodynamic indices for restenosis prediction. Comput Methods Programs Biomed. https://doi.org/10.1016/j.cmpb.2024.108214

Ouwendijk R, De Vries M, Pattynama PMT, Van Sambeek MRHM, De Haan MW, Stijnen T, Van Engelshoven JMA, Hunink MGM (2005) Imaging peripheral arterial disease: a randomized controlled trial comparing contrast-enhanced MR angiography and multi-detector row CT angiography. Radiology 236:1094–1103. https://doi.org/10.1148/radiol.2363041140

Owida AA, Do H, Morsi YS (2012) Numerical analysis of coronary artery bypass grafts: an over view. Comput Methods Programs Biomed 108:689–705. https://doi.org/10.1016/j.cmpb.2011.12.005

Piatti F, Sturla F, Bissell MM, Pirola S, Lombardi M, Nesteruk I, Votta E (2017) 4D flow analysis of BAV-Related fluid-dynamic alterations: Evidences of wall shear stress alterations in absence of clinically-relevant aortic anatomical remodeling. Front Physiol 8:441. https://doi.org/10.3389/fphys.2017.00441

Pinho N, Castro CF, António CC, Bettencourt N, Sousa LC, Pinto SIS (2019) Correlation between geometric parameters of the left coronary artery and hemodynamic descriptors of atherosclerosis: FSI and statistical study. Med Biol Eng Comput 57:715–729. https://doi.org/10.1007/s11517-018-1904-2

Poly(4-hydroxybutyrate), Polym. Database. (n.d.). https://polymerdatabase.com/polymers/Poly(4-hydroxybutyrate).html

Post A, Diaz-Rodriguez P, Balouch B, Paulsen S, Wu S, Miller J, Hahn M, Cosgriff-Hernandez E (2019) Elucidating the role of graft compliance mismatch on intimal hyperplasia using an ex vivo organ culture model. Acta Biomater 89:84–94. https://doi.org/10.1016/j.actbio.2019.03.025

Qiu Y, Tarbell JM (1996) Computational simulation of flow in the end-to-end anastomosis of a rigid graft and a compliant artery. ASAIO J. https://doi.org/10.1097/00002480-199609000-00078

Quicken S, de Bruin Y, Mees B, Tordoir J, Delhaas T, Huberts W (2020) Computational study on the haemodynamic and mechanical performance of electrospun polyurethane dialysis grafts. Biomech Model Mechanobiol 19:713–722. https://doi.org/10.1007/s10237-019-01242-1

Rabbi MF, Laboni FS, Arafat MT (2020) Computational analysis of the coronary artery hemodynamics with different anatomical variations. Inf Med Unlocked. https://doi.org/10.1016/j.imu.2020.100314

Rahmani S, Jarrahi A, Navidbakhsh M, Alizadeh M (2017) Investigating the performance of four specific types of material grafts and their effects on hemodynamic patterns as well as on von Mises stresses in a grafted three-layer aortic model using fluid-structure interaction analysis. J Med Eng Technol 41:630–643. https://doi.org/10.1080/03091902.2017.1382590

Ramachandra AB, Kahn AM, Marsden AL (2016) Patient-specific simulations reveal significant differences in mechanical stimuli in venous and arterial coronary grafts. J Cardiovasc Transl Res 9:279–290. https://doi.org/10.1007/s12265-016-9706-0

Rassoli A, Fatouraee N, Shafigh M (2015) Uniaxial and biaxial mechanical properties of the human saphenous vein. Biomed Eng Appl Basis Commun. https://doi.org/10.4015/S1016237215500507

Sankaranarayanan M, Chua LP, Ghista DN, Tan YS (2005) Computational model of blood flow in the aorto-coronary bypass graft. Biomed Eng Online. https://doi.org/10.1186/1475-925X-4-14

Savabi R, Nabaei M, Farajollahi S, Fatouraee N (2020) Fluid structure interaction modeling of aortic arch and carotid bifurcation as the location of baroreceptors. Int J Mech Sci. https://doi.org/10.1016/j.ijmecsci.2019.105222

Schiavone A, Zhao LG (2015) A study of balloon type, system constraint and artery constitutive model used in finite element simulation of stent deployment. Mech Adv Mater Mod Process. https://doi.org/10.1186/s40759-014-0002-x

Schoenborn S, Pirola S, Woodruff MA, Allenby MC (2022) Fluid-structure interaction within models of patient-specific arteries: computational simulations and experimental validations. IEEE Rev Biomed Eng. https://doi.org/10.1109/RBME.2022.3215678

Schoenborn S, Lorenz T, Kuo K, Fletcher DF, Woodruff MA, Pirola S, Allenby MC (2023) Fluid-structure interactions of peripheral arteries using a coupled in silico and in vitro approach. Comput Biol Med. https://doi.org/10.1016/j.compbiomed.2023.107474

Shav D, Gotlieb R, Zaretsky U, Elad D, Einav S (2014) Wall shear stress effects on endothelial-endothelial and endothelial-smooth muscle cell interactions in tissue engineered models of the vascular wall. PLoS ONE. https://doi.org/10.1371/journal.pone.0088304

Shu J, Santulli G (2018) Update on peripheral artery disease: epidemiology and evidence-based facts. Atherosclerosis 275:379–381. https://doi.org/10.1016/j.atherosclerosis.2018.05.033

Sottiurai VS, Yao JST, Flinn WR, Batson RC (1983) Intimal hyperplasia and neointima: an ultrastructural analysis of thrombosed grafts in humans. Surgery 93:809–817

Stansby G, Knez P, Berwanger CS, Nelson K, Reichert V, Schmitz-Rixen T (2001) Does vascular stapling improve compliance of vascular anastomoses? Vasc Endovascular Surg 35:115–121. https://doi.org/10.1177/153857440103500206

Stewart SFC, Lyman DJ (2004) Effects of an artery/vascular graft compliance mismatch on protein transport: a numerical study. Ann Biomed Eng 32:991–1006. https://doi.org/10.1023/B:ABME.0000032462.56207.65

Sugiyama SI, Niizuma K, Nakayama T, Shimizu H, Endo H, Inoue T, Tominaga T (2013) Relative residence time prolongation in intracranial aneurysms: a possible association with atherosclerosis. Neurosurgery 73(5):767–776

Suture Sizes and Suggested Indications for their use (2015) Oxford, 2–3. https://oxfordmedicaleducation.com/surgery/suture-sizes-and-suggested-indications-for-their-use/

Tai NR, Salacinski HJ, Edwards A, Hamilton G, Seifalian AM (2000) Compliance properties of conduits used in vascular reconstruction. Br J Surg 87:1516–1524. https://doi.org/10.1046/j.1365-2168.2000.01566.x

Taylor RS, McFarland RJ, Cox MI (1987) An investigation into the causes of failure of PTFE grafts. Eur J Vasc Endovasc Surg 1:335–343. https://doi.org/10.1016/S0950-821X(87)80061-0

Teng Z, Wang S, Tokgoz A, Taviani V, Bird J, Sadat U, Huang Y, Patterson AJ, Figg N, Graves MJ, Gillard JH (2021) Study on the association of wall shear stress and vessel structural stress with atherosclerosis: an experimental animal study. Atherosclerosis 320:38–46. https://doi.org/10.1016/j.atherosclerosis.2021.01.017

Thomas LV, Lekshmi V, Nair PD (2013) Tissue engineered vascular grafts: preclinical aspects. Int J Cardiol 167:1091–1100. https://doi.org/10.1016/j.ijcard.2012.09.069

Tiwari A, Cheng KS, Salacinski H, Hamilton G, Seifalian AM (2003) Improving the patency of vascular bypass grafts: the role of suture materials and surgical techniques on reducing anastomotic compliance mismatch. Eur J Vasc Endovasc Surg 25:287–295. https://doi.org/10.1053/ejvs.2002.1810

Trubel W, Schima H, Moritz A, Raderer F, Windisch A, Ullrich R, Windberger U, Losert U, Polterauer P (1995) Compliance mismatch and formation of distal anastomotic intimal hyperplasia in externally stiffened and lumen-adapted venous grafts. Eur J Vasc Endovasc Surg 10:415–423. https://doi.org/10.1016/S1078-5884(05)80163-7

Tubaldi E, Païdoussis MP, Amabili M (2018) Nonlinear dynamics of dacron aortic prostheses conveying pulsatile flow. J Biomech Eng. https://doi.org/10.1115/1.4039284

Van Bakel TMJ, Arthurs CJ, Nauta FJH, Eagle KA, Van Herwaarden JA, Moll FL, Trimarchi S, Patel HJ, Figueroa CA (2019) Cardiac remodelling following thoracic endovascular aortic repair for descending aortic aneurysms. Eur J Cardiothorac Surg 55:1061–1070. https://doi.org/10.1093/ejcts/ezy399

Vimmr J, Jonášová A (2010) Non-newtonian effects of blood flow in complete coronary and femoral bypasses. Math Comput Simul 80:1324–1336. https://doi.org/10.1016/j.matcom.2009.01.004

Walpoth BH, Bowlin GL (2005) The daunting quest for a small diameter vascular graft. Expert Rev Med Devices 2:647–651. https://doi.org/10.1586/17434440.2.6.647

Wang J, Paritala PK, Mendieta JB, Komori Y, Raffel OC, Gu Y, Li Z (2020) Optical coherence tomography-based patient-specific coronary artery reconstruction and fluid–structure interaction simulation. Biomech Model Mechanobiol 19:7–20. https://doi.org/10.1007/s10237-019-01191-9

Wang D, Serracino-Inglott F, Feng J (2021) Numerical simulations of patient-specific models with multiple plaques in human peripheral artery: a fluid-structure interaction analysis. Biomech Model Mechanobiol 20:255–265. https://doi.org/10.1007/s10237-020-01381-w

Yao G, Li H, Zuo X, Wang C, Xiao Y, Zhao Y, Wang X (2023) Oscillatory shear stress promotes vein graft intimal hyperplasia via NADPH oxidase-related pathways. Front Surg. https://doi.org/10.3389/fsurg.2023.1073557

Publisher's Note Springer Nature remains neutral with regard to jurisdictional claims in published maps and institutional affiliations.

Springer Nature or its licensor (e.g. a society or other partner) holds exclusive rights to this article under a publishing agreement with the author(s) or other rightsholder(s); author self-archiving of the accepted manuscript version of this article is solely governed by the terms of such publishing agreement and applicable law.